

# Finite-Size Critical Behavior of the Driven Lattice Gas

Sergio Caracciolo and Andrea Gambassi

*Scuola Normale Superiore and INFN – Sezione di Pisa  
I-56100 Pisa, ITALIA*

Internet: [sergio.caracciolo@sns.it](mailto:sergio.caracciolo@sns.it), [andrea.gambassi@sns.it](mailto:andrea.gambassi@sns.it)

Massimiliano Gubinelli

*Dipartimento di Fisica and INFN – Sezione di Pisa  
Università degli Studi di Pisa  
I-56100 Pisa, ITALIA*

Internet: [mgubi@cibs.sns.it](mailto:mgubi@cibs.sns.it)

Andrea Pelissetto

*Dipartimento di Fisica and INFN – Sezione di Roma I  
Università degli Studi di Roma “La Sapienza”  
I-00185 Roma, ITALIA*

Internet: [Andrea.Pelissetto@roma1.infn.it](mailto:Andrea.Pelissetto@roma1.infn.it)

November 1, 2018

## Abstract

We present a detailed Monte Carlo study of the high-temperature phase of the two-dimensional driven lattice gas at infinite driving field. We define a finite-volume correlation length, study its finite-size-scaling behavior and extrapolate it to the infinite-volume limit by using an iterative extrapolation method. The same method is applied to the susceptibility. We determine the transverse exponents  $\gamma$  and  $\nu$ . They turn out to be in perfect agreement with the theoretical predictions. We also compute the transverse Binder parameter, which apparently vanishes at the critical point, and the distribution of the magnetization. These results confirm the Gaussian nature of the transverse excitations.

# 1 Introduction

At present, the statistical mechanics of systems in thermal equilibrium is quite well established. On the other hand, little is known in general for non-equilibrium systems. It seems therefore worthwhile to study simple models which are out of thermal equilibrium. One of such systems is the model introduced at the beginning of the eighties by Katz, Lebowitz, and Spohn [1], who studied the stationary state of a lattice gas under the action of an external drive. The model, hereafter called *driven lattice gas* (DLG), is a kinetic Ising model on a periodic domain with Kawasaki dynamics and biased jump rates. Although not in thermal equilibrium, the DLG has a time-independent stationary state and shows a finite-temperature transition, which is however different in nature from its equilibrium counterpart [2].

Despite its simplicity, the DLG has not been solved exactly [3]. Nonetheless, many results have been obtained by means of Monte Carlo (MC) simulations and by using field-theoretical methods. In particular, Refs. [4, 5] developed a continuum model which is believed to capture the basic features of the transition and which provides exact predictions for the critical exponents [6]. Several computer simulations studied the critical behavior of these systems in two and three dimensions [7–10]. These simulations provided good support to the field-theoretical predictions, once it was understood that the highly anisotropic character of the transition required some kind of anisotropic finite-size scaling (FSS). Some attempts to formulate a phenomenological FSS theory can be found in Refs. [8, 11].

In spite of the extensive numerical work, there are no direct studies of the correlation length so far, essentially because it is not easy to define it. Indeed, in the high-temperature phase the model shows long-range correlations due to the violation of detailed balance [12, 13]. Therefore, no correlation length can be defined from the large-distance behavior of the two-point correlation function. A different definition is therefore necessary: in Refs. [14] a parallel correlation length is defined. However, this definition suffers from many ambiguities (see the discussion in Ref. [15]) and gives results for the exponent  $\nu_{\parallel}$  which are not in agreement with the theory [7]. Even more difficult appears the definition of a transverse correlation length because of the presence of negative correlations at large distances [7, 15].

In this paper we will define a finite-volume transverse correlation length generalizing the definition of the second-moment correlation length that is used in equilibrium systems. Because of the conserved dynamics, such a generalization requires some care. Here, we will use the results of Ref. [16].

Once a finite-volume correlation length is defined, we can use the method of Ref. [17] to determine infinite-volume quantities [18]. Such a method is particularly efficient and it has been applied successfully to many different models [19–25]. Once the infinite-volume quantities have been computed, we can determine the critical exponents by analyzing the singularities in the limit  $T \rightarrow T_c$ .

The paper is organized as follows. In Sec. 2 we describe the model and define the observables measured in the MC simulation. Section 3 reviews the FSS theory and introduces the basic formulae that are used in the analysis of the simulations. Next in Sec. 4, we consider the field-theoretical model of Refs. [4, 5] in a finite geometry and compute the

FSS functions for several observables. In Sec. 5 we describe the simulations and present the results which are then discussed in Sec. 6. We confirm the field-theoretical predictions with good precision both for infinite-volume quantities and for the finite-size behavior at the critical point. Our results also indicate that the transverse Binder parameter vanishes at the critical point, in agreement with the idea that transverse modes are purely Gaussian.

## 2 Definitions

### 2.1 The model

As a prelude to the DLG consider a simple lattice gas of interacting particles. We consider a finite square lattice  $\Lambda$  and  $N$  particles, each of them occupying a different lattice site. A configuration of the system is specified by the set of occupation numbers of each site  $n = \{n_i \in \{0, 1\}\}_{i \in \Lambda}$ . We assume a nearest-neighbor attractive (“ferromagnetic” in spin language) Hamiltonian

$$H_\Lambda[n] = -J \sum_{\langle i,j \rangle \in \Lambda} n_i n_j, \quad (1)$$

where  $J > 0$  (in the following we will set without loss of generality  $J = 1$ ) and the sum runs over all lattice nearest neighbors. We consider a discrete-time Kawasaki-type dynamics [26], which preserves the total number of particles  $N$  or, equivalently, the density

$$\rho_\Lambda \equiv \frac{1}{|\Lambda|} \sum_{i \in \Lambda} n_i, \quad (2)$$

where  $|\Lambda|$  is the total number of sites in  $\Lambda$ . At each step, we choose randomly a lattice link  $\langle i, j \rangle$ . If  $n_i = n_j$ , nothing happens. Otherwise, we propose a swap, i.e. a particle jump, with probability  $w(\Delta H/T)$ , where

$$\Delta H = H_\Lambda[n'] - H_\Lambda[n] \quad (3)$$

is the difference in energy between the new ( $n'$ ) and the old ( $n$ ) configuration. If the probability  $w(x)$  satisfies

$$w(-x) = e^x w(x), \quad (4)$$

then the dynamics is reversible, i.e. satisfies detailed balance. Under these conditions there is a unique equilibrium measure given by the Gibbs one

$$P_{\Lambda,eq}[n] = \frac{e^{-\beta H_\Lambda[n]}}{\sum_{\{n'\}} e^{-\beta H_\Lambda[n']}}, \quad (5)$$

where  $\beta \equiv 1/T$ . In the thermodynamic limit, i.e.  $|\Lambda| \rightarrow \infty$ , the lattice gas exhibits a second-order phase transition for  $\rho_\Lambda = 1/2$  at the Onsager value  $\beta_c = \frac{1}{2} \ln(\sqrt{2} + 1)$ .

The DLG is a generalization of the lattice gas in which one introduces a uniform (in space and time) force field pointing along one of the axes of the lattice, i.e.  $\mathbf{E} = E\hat{\mathbf{x}}$ : It favors (respectively suppresses) the jumps of the particles in the positive (resp. negative)

$\hat{\mathbf{x}}$ -direction. If  $\Lambda$  is bounded by *rigid walls*, then  $\mathbf{E}$  is a conservative field and it can be accounted for by adding a potential term to  $H_\Lambda[n]$ . Therefore, the system remains in thermal equilibrium: the net effect of  $\mathbf{E}$  is simply to induce a concentration gradient in the equilibrium state.

Here, we will consider instead periodic boundary conditions [27]. In this case, the field  $\mathbf{E}$  does not have a global potential and the system reaches a stationary state which, however, is not a state in thermal equilibrium.

In the DLG transition probabilities take into account the work done by the field during the particle jump from one site to one of its nearest neighbors. In this case one proposes a particle jump with probability  $w(\beta \Delta H + \beta E \ell)$ , with  $\ell = (1, 0, -1)$  for jumps (along, transverse, opposite) to  $\hat{\mathbf{x}}$ .

For  $E \neq 0$  and  $\rho_\Lambda = 1/2$ , the system shows a continuous phase transition at an inverse temperature  $\beta_c(E)$  which saturates, for  $E \rightarrow \infty$ , at  $\beta_c(\infty) \approx 0.71\beta_c(0)$ . For  $\beta < \beta_c(E)$  particles are homogeneously distributed in space, while for  $\beta > \beta_c(E)$  the gas separates in two regions, one almost full and the other almost empty, with interfaces parallel to  $\mathbf{E}$ .

## 2.2 Observables

We consider a finite square lattice of size  $L_\parallel \times L_\perp$  with periodic boundary conditions. We define a “spin” variable  $s_j \equiv 2n_j - 1$  and its Fourier transform

$$\phi(\mathbf{k}) \equiv \sum_{j \in \Lambda} e^{i\mathbf{k} \cdot \mathbf{j}} s_j, \quad (6)$$

where the allowed momenta are

$$\mathbf{k}_{n,m} \equiv \left( \frac{2\pi n}{L_\parallel}, \frac{2\pi m}{L_\perp} \right), \quad (7)$$

with  $(n, m) \in \mathbb{Z}_{L_\parallel} \times \mathbb{Z}_{L_\perp}$ .

We consider the model at half filling, i.e. for  $\rho_\Lambda = 1/2$ . Then

$$\sum_{j \in \Lambda} s_j = 0, \quad \text{i.e.} \quad \phi(\mathbf{k}_{0,0}) = 0. \quad (8)$$

In the ordered phase  $|\phi(\mathbf{k})|$  takes its maximum for  $\mathbf{k} = \mathbf{k}_{0,1}$ , and the expectation value on the steady state of its module

$$m(L_\parallel, L_\perp) \equiv \frac{1}{|\Lambda|} \langle |\phi(\mathbf{k}_{0,1})| \rangle \quad (9)$$

is a good order parameter.

In momentum space the static structure factor

$$\tilde{G}(\mathbf{k}; L_\parallel, L_\perp) \equiv \frac{1}{|\Lambda|} \langle |\phi(\mathbf{k})|^2 \rangle \quad (10)$$

vanishes at  $\mathbf{k}_{0,0}$  because of Eq. (8) and is maximal at  $\mathbf{k}_{0,1}$ , so that it is natural to define the susceptibility as [29]

$$\chi(L_\parallel, L_\perp) \equiv \tilde{G}(\mathbf{k}_{0,1}; L_\parallel, L_\perp). \quad (11)$$

Another interesting observable is the transverse Binder's cumulant  $g(L_{\parallel}, L_{\perp})$  defined as

$$g(L_{\parallel}, L_{\perp}) \equiv 2 - \frac{\langle |\phi(\mathbf{k}_{0,1})|^4 \rangle}{\langle |\phi(\mathbf{k}_{0,1})|^2 \rangle^2}. \quad (12)$$

Next, we would like to define a correlation length. In infinite-volume equilibrium systems there are essentially two different ways of doing it. One can define the correlation length in terms of the large-distance behavior of the two-point function or by using the small-momenta behavior of the two-point function (second-moment correlation length). In the DLG the first method does not work. Indeed, in the high-temperature phase the two-point function  $\langle s_{\mathbf{x}} s_{\mathbf{0}} \rangle$  always decays *algebraically* with the distance even in the high-temperature phase. Moreover, it is not positive definite because of negative correlations in the transverse directions [15]. This peculiar behavior is due to the fact that in the infinite-volume limit (at fixed temperature) the static structure factor  $\tilde{G}(\mathbf{k}; \infty, \infty)$  has a finite discontinuity at  $\mathbf{k} = 0$ .

To overcome the difficulties of the real-space strategy we will define the correlation length by using the two-point function for small momenta. We follow Ref. [16], where we discussed the possible definitions of correlation length in the absence of the zero mode, as it is the case here.

We consider the structure factor in finite volume at zero longitudinal momenta

$$\tilde{G}_{\perp}(q; L_{\parallel}, L_{\perp}) \equiv \tilde{G}((0, q); L_{\parallel}, L_{\perp}), \quad (13)$$

(note that the conservation law implies  $\tilde{G}_{\perp}(0; L_{\parallel}, L_{\perp}) = 0$ ) and introduce a finite-volume (transverse) correlation length

$$\xi_{ij}(L_{\parallel}, L_{\perp}) \equiv \sqrt{\frac{1}{\hat{q}_j^2 - \hat{q}_i^2} \left( \frac{\tilde{G}_{\perp}(q_i; L_{\parallel}, L_{\perp})}{\tilde{G}_{\perp}(q_j; L_{\parallel}, L_{\perp})} - 1 \right)}, \quad (14)$$

where  $\hat{q}_n = 2 \sin(\pi n / L_{\perp})$  is the lattice momentum.

Some comments are in order:

- (i) If we consider an equilibrium system or a steady state in which correlations decay exponentially, then we have for  $q \rightarrow 0$  that

$$\tilde{G}_{\perp}^{-1}(q; L_{\parallel}, L_{\perp}) = \chi(L_{\parallel}, L_{\perp})^{-1} (1 + \xi_{ij}^2(L_{\parallel}, L_{\perp}) q^2 + O(q^4, L^{-2})). \quad (15)$$

where  $\chi(L_{\parallel}, L_{\perp})$  is the susceptibility. Thus,  $\xi_{ij}^2(\infty, \infty)$  is a good definition of correlation length which has an infinite-volume limit independent of  $i$  and  $j$ .

- (ii) Since  $\tilde{G}_{\perp}(0; L_{\parallel}, L_{\perp}) = 0$ ,  $q_i$  and  $q_j$  must not vanish. Moreover, as discussed in Ref. [16], the definition should be valid for all  $T$  in finite volume. Since the system orders in an even number of stripes, for  $i$  even  $\tilde{G}_{\perp}(q_i; L_{\parallel}, L_{\perp}) = 0$  is zero as  $T \rightarrow 0$ . Therefore, if our definition should capture the nature of the phase transition, we must require  $i$  and  $j$  to be odd. Although any choice of  $i, j$  is conceptually good, finite-size corrections increase with  $i, j$ , a phenomenon which should be expected since the critical modes correspond to  $q \rightarrow 0$ . Thus, we will choose  $(i, j) = (1, 3)$ .

For a more thorough discussion of the definition (14), which is mainly motivated by the absence of the zero mode, we refer to Ref. [16] where its finite-size behavior is studied in the context of the large- $N$  approximation of the  $N$ -vector model.

Another quantity which is considered in the analysis is the amplitude  $A_{13}$  defined by

$$A_{13}(L_{\parallel}, L_{\perp}) \equiv \frac{\xi_{13}^2}{\chi}. \quad (16)$$

### 3 Finite-size scaling

In the neighborhood of a critical point the behavior of long-range observables is controlled by few quantities, corresponding in the renormalization-group language to coordinates parametrizing the relevant directions. When the system is finite, its size can be effectively incorporated in the scaling analysis as another relevant operator. This means that an observable  $\mathcal{O}$ , which diverges in the thermodynamic limit as

$$\mathcal{O}_{\infty}(\beta) \sim t^{-\gamma_{\mathcal{O}}} \quad \text{for } t \equiv 1 - \frac{\beta}{\beta_c} \rightarrow 0^+, \quad (17)$$

behaves in an isotropic finite system of linear size  $L$  as

$$\mathcal{O}_L(\beta) \approx t^{-\gamma_{\mathcal{O}}} F_{1,\mathcal{O}}(t^{-\nu}/L) \approx L^{\gamma_{\mathcal{O}}/\nu} F_{2,\mathcal{O}}(t^{-\nu}/L) \approx L^{\gamma_{\mathcal{O}}/\nu} F_{3,\mathcal{O}}(\xi_{\infty}/L), \quad (18)$$

where  $\xi_{\infty}(\beta)$  is the infinite-volume correlation length. From Eq. (18) we can derive a general relation for the ratio of  $\mathcal{O}_L$  at two different sizes  $L$  and  $\alpha L$ :

$$\frac{\mathcal{O}_{\alpha L}(\beta)}{\mathcal{O}_L(\beta)} = F_{\mathcal{O}}\left(\frac{\xi_L(\beta)}{L}\right), \quad (19)$$

where we have traded  $\xi_{\infty}/L$  for  $\xi_L/L$  by inverting  $\xi_L \approx L F_{3,\xi}(\xi_{\infty}/L)$ .

The function  $F_{\mathcal{O}}(z)$  is universal and is directly accessible numerically, e.g., by MC simulations. It depends on  $\alpha$  and, for a two-dimensional finite lattice of dimension  $L_{\perp} \times L_{\parallel}$ , on the ratio  $L_{\perp}/L_{\parallel}$ . The appropriate FSS limit is indeed achieved by taking the limit  $L_{\perp}, L_{\parallel}, \xi_L \rightarrow \infty$  with  $L_{\perp}/L_{\parallel}$  and  $\xi_L/L$  fixed.

If we define  $z = \xi_L/L$ , then  $z$  varies between 0 and  $z^*$ , where  $z^*$  is defined by

$$z^* = F_{3,\xi}(\infty). \quad (20)$$

The value  $z^*$  is directly related to the behavior of the finite-size correlation length at the critical point, since  $\xi_L(\beta_c) \approx z^*L$ . For ordinary phase transitions  $z^*$  is finite. At the critical point it also holds

$$\mathcal{O}_L(\beta_c) \propto L^{\gamma_{\mathcal{O}}/\nu}. \quad (21)$$

Then

$$F_{\mathcal{O}}(z^*) = \frac{\mathcal{O}_{\alpha L}(\beta_c)}{\mathcal{O}_L(\beta_c)} = \alpha^{\gamma_{\mathcal{O}}/\nu}, \quad (22)$$

and therefore

$$\frac{\gamma_{\mathcal{O}}}{\nu} = \frac{\log F_{\mathcal{O}}(z^*)}{\log \alpha}. \quad (23)$$

The above-presented results are valid for an isotropic system. On the other hand, there are clear numerical evidences that the phase transition in the DLG model is strongly anisotropic. The continuum field theories introduced to describe the critical singularities predict a nontrivial *anisotropy exponent*  $\Delta$ . For example, the scaling form of the critical two-point function is predicted to be

$$\tilde{G}(k_{\perp}, k_{\parallel}) \approx \mu^{-2+\eta} \tilde{G}(\mu k_{\perp}, \mu^{1+\Delta} k_{\parallel}), \quad (24)$$

where  $\eta$  is the anomalous dimension of the density field.

It is then natural to assume the existence of two correlation lengths  $\xi_{\perp}, \xi_{\parallel}$  which diverge with different exponents  $\nu_{\perp}$  and  $\nu_{\parallel}$  related by

$$\nu_{\parallel} = (1 + \Delta)\nu_{\perp}. \quad (25)$$

These considerations call for an extension of the FSS arguments. A phenomenological approach to FSS for the DLG has been developed [14], keeping into account the strong anisotropy observed in the transition (for  $d = 2$  see Refs. [8,9,11], for  $d = 3$  see Refs. [10]). Following this approach, we assume that all observables have a finite FSS limit obtained by taking the longitudinal size  $L_{\parallel}$  and the transverse size  $L_{\perp}$  to infinity keeping constant:

- the *anisotropic aspect ratio*  $S = S_{\Delta} \equiv L_{\parallel}^{1/(1+\Delta)}/L_{\perp}$ ;
- the *FSS parameter*  $\xi_{\perp,\infty}(\beta)/L_{\perp}$  (or equivalently its longitudinal counterpart).

Then, Eq. (18) still holds by using the correct FSS parameter. Using transverse quantities we rewrite

$$\mathcal{O}_L(\beta) \approx t^{-\gamma_{\mathcal{O}}} F_{1,\mathcal{O}}(t^{-\nu_{\perp}}/L_{\perp}) \approx L_{\perp}^{\gamma_{\mathcal{O}}/\nu_{\perp}} F_{2,\mathcal{O}}(t^{-\nu_{\perp}}/L_{\perp}) \approx L_{\perp}^{\gamma_{\mathcal{O}}/\nu_{\perp}} F_{3,\mathcal{O}}(\xi_{\perp,\infty}/L_{\perp}). \quad (26)$$

Analogously Eq. (19) is recast in the form

$$\frac{\mathcal{O}_{\alpha L_{\perp}}(\beta, S)}{\mathcal{O}_{L_{\perp}}(\beta, S)} = F_{\mathcal{O}}\left(\frac{\xi_{\perp,L_{\perp}}(\beta)}{L_{\perp}}, \alpha, S\right). \quad (27)$$

where we have shown explicitly the dependence on  $\alpha$  and on the aspect ratio  $S$ . Equation (27) will be the basis for our analysis of the phase transition in the DLG. For the transverse finite-volume correlation length we will use  $\xi_{13}$  as defined in Sec. 2.2. Moreover, as much of our efforts are aimed to test accurately the theoretical predictions of Refs. [4,5], we *assume* that  $\Delta = 2$  for  $d = 2$  and in the sequel we always consider  $S \equiv S_2$ .

## 4 Field-theory description of the DLG

As we explained in Sec. 2.1, the DLG is a lattice gas model. However, in a neighborhood of the critical point (critical region) we can limit ourselves to consider slowly-varying (in space and time) observables. At criticality the lattice spacing is negligible compared to the length and time scales at which long-range order is established so that it is possible to formulate a description of the system in terms of *mesoscopic* variables. In principle, the

dynamics of such variables can be obtained by coarse graining the microscopic system. However, given the difficulty of performing a rigorous coarse-graining procedure, one postulates a continuum field theory that preserves all symmetries of the microscopic lattice model. By universality the continuum model should have the same critical behavior of the microscopic one. In this framework a field theory has been proposed [4, 5, 28] (see also Ref. [15]) and analyzed, giving rise to exact predictions for the critical exponents in space dimension  $d$  with  $2 < d < 5$ .

The starting point of the theory is the dynamic functional [30–32] which reads (neglecting terms which are irrelevant by power counting) [4, 5]

$$J[s, \tilde{s}] = \int d^d \mathbf{x} dt \lambda \left\{ \tilde{s} [\lambda^{-1} \partial_t + \Delta_{\perp} (\Delta_{\perp} - \tau) - \rho \Delta_{\parallel}] s + \frac{1}{2} u_0 \nabla_{\parallel} \tilde{s} s^2 + \tilde{s} \Delta_{\perp} \tilde{s} \right\}, \quad (28)$$

where  $s(\mathbf{x}, t)$  is the local density field (coarse-grained version of  $s_i$ ),  $\tilde{s}$  is the response field,  $\tau$  is the effective distance from the critical point,  $\rho$  is a parameter, and  $u_0$  is the coupling-constant of the theory which takes into account the leading effects of the microscopic force field. A careful analysis shows that only the parameter  $\rho$  needs to be renormalized, allows to determine the upper critical dimension, which turns out to be  $d_c = 5$ , and gives exact predictions for the critical exponents [4, 5].

For the structure factor the renormalization-group analysis gives the scaling form

$$\tilde{G}(k_{\parallel}, k_{\perp}; \tau) = \mu^{-2+\eta} \tilde{G}(k_{\parallel} \mu^{-1-\Delta}, k_{\perp} \mu^{-1}; \tau \mu^{-1/\nu}), \quad (29)$$

where, in  $d$  dimensions,

$$\eta = 0, \quad (30)$$

$$\nu = \frac{1}{2}, \quad (31)$$

$$\Delta = \frac{1}{3}(8 - d), \quad (32)$$

and  $\tau \propto T - T_c$ . In two dimensions, for the transverse structure factor, this implies the simple scaling form

$$\tilde{G}_{\perp}(k; \tau) = \tau^{-1} f(k^2/\tau). \quad (33)$$

Thus, in infinite volume we have

$$\xi_{ij} \sim \tau^{-\nu}, \quad \chi \sim \tau^{-\gamma}, \quad (34)$$

where  $\nu$  is given in Eq. (31) and

$$\gamma = 1. \quad (35)$$

The function  $f(x)$  defined in Eq. (33) is trivial. Indeed, keeping into account causality and the form of the interaction vertex one can see that for  $k_{\parallel} = 0$  there are no loop contributions to the two-point function (and also to the response function  $\langle \tilde{s}_0 s_x \rangle$ ). Thus, for all  $2 \leq d \leq 5$ ,  $\tilde{G}_{\perp}(k, \tau)$  is simply given by the tree-level expression

$$\tilde{G}_{\perp}(k; \tau) = \frac{1}{k^2 + \tau}. \quad (36)$$



Two observations are here in order. First,  $\tau$  is an analytic function of  $t$  such that  $\tau = 0$  for  $t = 0$ ; thus,  $\tau = bt$  for  $t \rightarrow 0$  with  $b$  positive constant. Second, the function that appears in Eq. (36) refers to the coarse-grained fields, which, in the critical limit, differ by a finite renormalization from the lattice ones. Thus, for the lattice function we are interested in, in the scaling limit  $t \rightarrow 0$ ,  $k \rightarrow 0$ , with  $k^2/t$  fixed, we have

$$\tilde{G}_{\perp,\text{latt}}(k; t) = \frac{Z}{k^2 + bt}, \quad (37)$$

where  $Z$  and  $b$  are positive constants.

On the same footing, we can conclude that all correlation functions with vanishing longitudinal momenta behave as in a free theory. In particular, the Binder cumulant defined in Eq. (12) vanishes. It is also important to notice that Eq. (37) implies the exponential decay of

$$G_{\perp,\text{latt}}(x_{\perp}; t) = \int d^{d-1}k e^{ikx_{\perp}} \tilde{G}_{\perp,\text{latt}}(k; t), \quad (38)$$

which fully justifies our definition of transverse correlation length.

In this paper, we will study the FSS behavior of the model. Here, we want to analyze the corresponding continuum field theory in a finite geometry following the method applied in equilibrium spin systems (see, e.g., Ref. [33, Chap. 36] and references therein). The idea is quite simple. Consider the system in a finite box with periodic boundary conditions. The finite geometry has the only effect of quantizing the momenta. Thus, the perturbative finite-volume correlation functions are obtained by replacing momentum integrals by lattice sums. Ultraviolet divergences are not affected by the presence of the box [34] and thus one can use the infinite-volume renormalization constants. Once the renormalization is carried out, one obtains the geometry-dependent finite-size correlation functions.

Following this idea, if we consider a finite box of size  $L_{\parallel} \times L_{\perp}$ , Eq. (29) becomes

$$\tilde{G}(k_{\parallel}, k_{\perp}; \tau; L_{\parallel}, L_{\perp}) = \mu^{-2} \tilde{G}(k_{\parallel} \mu^{-1-\Delta}, k_{\perp} \mu^{-1}; \tau \mu^{-2}; L_{\parallel} \mu^{-1-\Delta}, L_{\perp} \mu^{-1}), \quad (39)$$

which shows that at  $T = T_c$

$$\xi_{ij}(T_c) \sim L_{\perp}, \quad \chi(T_c) \sim L_{\perp}^{\gamma/\nu} \sim L_{\perp}^2. \quad (40)$$

Moreover, Eq. (36) holds in finite volume. Keeping again into account the relation between coarse-grained and lattice quantities, we obtain for the lattice correlation function in a finite volume in the continuum limit (i.e. in the FSS limit with  $k \rightarrow 0$  keeping  $k^2/t$  fixed)

$$\tilde{G}_{\perp,\text{latt}}(k; t; L_{\parallel}, L_{\perp}) = \frac{Z(t; L_{\parallel}, L_{\perp})}{k^2 + \tau(t; L_{\parallel}, L_{\perp})}, \quad (41)$$

where  $Z$  and  $\tau$  are analytic functions of their arguments. In the FSS limit, we expect

$$Z(t; L_{\parallel}, L_{\perp}) = \tilde{Z}(tL_{\perp}^2, S_{\Delta}), \quad (42)$$

$$\tau(t; L_{\parallel}, L_{\perp}) = L_{\perp}^{-2} \tilde{\tau}(tL_{\perp}^2, S_{\Delta}). \quad (43)$$

Using these expressions, in the FSS limit we find

$$\frac{\xi_{13}(t; L_{\parallel}, L_{\perp})}{L_{\perp}} = ((2\pi)^2 + \tilde{\tau}(tL_{\perp}^2, S_{\Delta}))^{-1/2}, \quad (44)$$

$$A_{13} \equiv \frac{\xi_{13}^2(t; L_{\parallel}, L_{\perp})}{\chi(t; L_{\parallel}, L_{\perp})} = \left[ \tilde{Z}(tL_{\perp}^2, S_{\Delta}) \right]^{-1}, \quad (45)$$

valid for  $t \rightarrow 0$ ,  $L_{\parallel}, L_{\perp} \rightarrow \infty$  with  $S_2$  and  $tL_{\perp}^2$  fixed. Therefore, from the scaling of the correlation length and of the amplitude  $A_{13}$  we can derive the scaling functions  $\tilde{Z}$  and  $\tilde{\tau}$ .

If we make the simplest approximations  $\tilde{Z}(tL_{\perp}^2, S_{\Delta}) = \text{const}$  and  $\tilde{\tau}(tL_{\perp}^2, S_{\Delta}) = \text{const} \times tL_{\perp}^2$ , we obtain for the scaling functions defined in Eq. (27) the approximate forms

$$F_{\xi}(z) = [1 - (1 - \alpha^{-2})(2\pi)^2 z^2]^{-1/2}, \quad (46)$$

$$F_{\chi}(z) = F_{\xi}^2(z) = [1 - (1 - \alpha^{-2})(2\pi)^2 z^2]^{-1}. \quad (47)$$

As we shall see, these expressions provide reasonably good approximations to our data, but do not describe the data exactly: The functions  $\tilde{\tau}$  and  $\tilde{Z}$  that are determined from the data are nontrivial.

In the previous discussion we have neglected the possible presence of a dangerously irrelevant operator that becomes marginal at  $d = 2$ . Its presence may modify the scaling relations (29), (33), and (39). Considering  $\tilde{G}_{\perp}(k)$  we have

$$\tilde{G}_{\perp}(k; \tau; L_{\parallel}, L_{\perp}; u) = \mu^{-2} \tilde{G}_{\perp}(k\mu^{-1}; \tau\mu^{-2}; L_{\parallel}\mu^{-1-\Delta}, L_{\perp}\mu^{-1}; u\mu^{2\sigma}), \quad (48)$$

where,  $\sigma = (d-2)/3$  in  $d$  dimensions, and  $u$  is the irrelevant coupling. If the scaling function vanishes for  $u \rightarrow 0$ , one obtains an anomalous scaling behavior. In two dimensions, since the operator is marginal ( $\sigma = 0$ ), we expect logarithmic corrections to the formulae previously computed. It is also possible that logarithmic terms modify Eq. (27). In the absence of any prediction, we will neglect these logarithmic violations. As it has been observed in previous numerical studies, if present, they are small [8]. As we will discuss, this is confirmed by our numerical results.

Finally, we want to notice that the Gaussian nature of the fields at zero longitudinal momenta allow us to write down the probability distribution of  $\phi(\mathbf{k}_{0,n})$ . Indeed, the previous results give

$$P(\phi(\mathbf{k}_{0,n})) = \frac{1}{N} \exp \left[ -\frac{1}{L_{\parallel}L_{\perp}} \phi(-\mathbf{k}_{0,n}) \tilde{G}_{\perp, \text{latt}}^{-1}(\mathbf{k}_{0,n}) \phi(\mathbf{k}_{0,n}) \right], \quad (49)$$

where  $N$  is a normalization factor. From this expression we can derive the probability distribution of  $M^2 = |\phi(\mathbf{k}_{0,1})|^2 / L_{\parallel}^2 L_{\perp}^2$ . Of course,  $\langle M \rangle = m$ ,  $\langle M^2 \rangle = \chi / (L_{\parallel}L_{\perp})$  (see Eqs. (9), (10), and (11)). We obtain

$$P(M^2) dM^2 = \frac{1}{\sigma^2} e^{-M^2/\sigma^2} dM^2, \quad (50)$$

where

$$\sigma^2 = \frac{1}{L_{\parallel}L_{\perp}} \tilde{G}_{\perp, \text{latt}}(2\pi/L_{\perp}) = \frac{1}{L_{\parallel}L_{\perp}} \chi(L_{\parallel}, L_{\perp}). \quad (51)$$

## 5 Numerical Simulation

### 5.1 Setup

We studied the phase transition of the DLG in two dimensions by MC simulations. Our aim was to check the validity of the FSS assumptions and eventually to use FSS to compute the critical exponents. The observables we took into account are those described in Sec. 2.2.

We used the dynamics described in Sec. 2.1 with Metropolis rates, i.e. we set

$$w(x) = \min(1, e^{-x}). \quad (52)$$

Simulations are performed at infinite driving field: therefore, forward (backward) jumps in the direction of the field are always accepted (rejected).

The dynamics of the DLG is diffusive with dynamic critical exponent [4]  $z = 4$ . Thus, it is important to have an efficient implementation of the dynamics in order to cope with the severe critical slowing down.

We use the random-number generator `ran_array` described in Ref. [35] in order to choose the links and to perform the Metropolis step and multi-spin coding techniques to evolve simultaneously many independent configurations. On 32-bit machines the state of a single site for 10 configurations is coded in a 32-bit word, using 3 bits per configuration. This peculiar allocation is useful when computing the number of occupied neighbors of a given site: Since this number is at most 4 in 2 dimensions we can use 32-bit arithmetics without overflow. The Metropolis step is coded in an entirely algebraic way avoiding branching instructions and taking full advantage of the pipelining capabilities of most microprocessors. On Pentium machines we achieved a speed of 0.01  $\mu$ sec for single spin flip, while our code performs a bit worse on Motorola *R10000* or Alpha processors but on these machines it is possible to simulate 21 systems using 64-bit integers.

We considered lattices with an approximately constant aspect ratio  $S_2 \approx 0.200$ . We sampled very accurately those with sizes  $(L_{\parallel}, L_{\perp})$  corresponding to (21, 14), (32, 16), (46, 18), (64, 20), (84, 22), (110, 24), (168, 28) for which  $S_2$  lies between 0.197 and 0.202. We checked that a change of  $\pm 1$  on  $L_{\parallel}$  has an effect on the observables that is negligible with respect to the statistical error. In the following we write  $L$  for  $L_{\perp}$ .

It is very important to be sure that the system has reached the steady-state distribution before sampling. Metastable configurations in which the chain could be trapped for times much longer than typical relaxation times in the steady state are a dangerous source of bias. In the DLG, configurations in which multiple stripes aligned with the external field are present are very long-lived and it is possible that they persist for times of the order of those of typical simulation runs, thus effectively inducing a spurious geometry on the system. To avoid the formation of stripes, we took care to initialize the larger systems by suitably rescaled thermalized configurations of smaller systems (where the stripes decay faster) at the same temperature and value of  $S_2$ .

We computed the autocorrelation time  $\tau_{\chi}$  for the susceptibility  $\chi$ . Such an observable is expected to have a significant overlap with the slowest modes of the system, so that  $\tau_{\chi}$  should give a good indication of the number of sweeps necessary to generate independent configurations. We found that, for the lowest temperature we considered ( $\beta = 0.311$ ),  $\tau_{\chi} \approx$

$L$	$\xi_{12}$	$\xi_{13}$	$\chi$	$A_{13}$	$m$	$g$
$\beta = 0.2700$						
14	1.3824(16)	1.3769(11)	8.0489(50)	0.23555(28)	0.148869(50)	0.20672(73)
16	1.4455(21)	1.4448(15)	8.8606(69)	0.23558(36)	0.117807(49)	0.1495(10)
18	1.4942(27)	1.4905(17)	9.4795(83)	0.23436(41)	0.095533(44)	0.1105(10)
20	1.5294(35)	1.5283(22)	9.960(10)	0.23450(51)	0.078584(43)	0.0786(13)
$\beta = 0.2750$						
14	1.4532(16)	1.4455(11)	8.7094(53)	0.23992(27)	0.155093(51)	0.22560(72)
16	1.5252(22)	1.5206(15)	9.6826(74)	0.23881(35)	0.123347(51)	0.16947(98)
18	1.5793(28)	1.5796(18)	10.4511(93)	0.23873(41)	0.100445(47)	0.1273(11)
20	1.6280(35)	1.6255(22)	11.073(12)	0.23862(49)	0.082940(46)	0.0923(13)
$\beta = 0.2800$						
14	1.5286(16)	1.5172(11)	9.4382(56)	0.24389(27)	0.161823(52)	0.25090(68)
16	1.6159(21)	1.6118(15)	10.6473(81)	0.24399(34)	0.129594(53)	0.19095(95)
18	1.6858(26)	1.6821(19)	11.641(10)	0.24304(40)	0.106178(49)	0.1473(10)
20	1.7428(34)	1.7408(22)	12.421(13)	0.24396(46)	0.087965(48)	0.1101(12)
$\beta = 0.2850$						
14	1.6086(16)	1.5940(11)	10.2434(60)	0.24803(26)	0.168977(54)	0.27700(65)
16	1.7152(21)	1.7048(15)	11.7579(87)	0.24719(33)	0.136493(54)	0.21965(88)
18	1.7998(27)	1.7963(19)	13.029(11)	0.24765(38)	0.112516(51)	0.16941(98)
20	1.8654(34)	1.8657(23)	14.067(15)	0.24745(45)	0.093766(51)	0.1334(12)
$\beta = 0.2900$						
14	1.6976(16)	1.6769(12)	11.1664(64)	0.25183(26)	0.176906(55)	0.30542(61)
16	1.8243(22)	1.8130(16)	13.0604(95)	0.25168(33)	0.144208(57)	0.24750(84)
18	1.9347(27)	1.9256(19)	14.729(12)	0.25174(37)	0.119924(54)	0.20021(91)
20	2.0225(34)	2.0137(24)	16.134(17)	0.25132(43)	0.100638(55)	0.1608(11)
22	2.0904(31)	2.0862(21)	17.310(15)	0.25142(38)	0.086542(40)	0.1292(11)
24	2.1457(35)	2.1447(23)	18.304(17)	0.25129(39)	0.074305(35)	0.1026(12)
28	2.2444(45)	2.2389(29)	19.900(22)	0.25190(46)	0.057904(33)	0.0685(14)
$\beta = 0.2950$						
14	1.7941(16)	1.7685(12)	12.2087(68)	0.25617(26)	0.185533(57)	0.33682(58)
16	1.9527(22)	1.9338(16)	14.602(10)	0.25609(32)	0.152967(58)	0.28268(78)
18	2.0893(27)	2.0740(20)	16.797(14)	0.25609(37)	0.128498(56)	0.23771(85)
20	2.2041(34)	2.1941(25)	18.754(19)	0.25670(41)	0.108808(60)	0.1956(10)
22	2.2962(32)	2.2878(22)	20.434(18)	0.25614(36)	0.094271(43)	0.1623(10)
24	2.3770(33)	2.3731(23)	21.937(19)	0.25671(35)	0.081524(36)	0.1315(10)
28	2.5045(50)	2.5028(33)	24.333(29)	0.25743(46)	0.064138(40)	0.0922(14)
$\beta = 0.2970$						
14	1.8368(16)	1.8072(12)	12.6676(70)	0.25783(26)	0.189260(58)	0.35048(57)
16	2.0076(22)	1.9852(16)	15.298(11)	0.25762(32)	0.156795(60)	0.29750(76)
18	2.1538(27)	2.1369(20)	17.709(15)	0.25786(35)	0.132092(58)	0.25094(84)
20	2.2786(36)	2.2698(26)	19.949(21)	0.25826(41)	0.112359(62)	0.2100(10)
22	2.3867(32)	2.3778(23)	21.940(19)	0.25771(35)	0.097791(45)	0.1773(10)
24	2.4838(33)	2.4787(24)	23.735(20)	0.25885(34)	0.084924(39)	0.1488(10)
28	2.6308(53)	2.6194(36)	26.590(34)	0.25804(46)	0.067096(45)	0.1030(14)

Table 1: Monte Carlo results.

900, 1400, 2700 sweeps, for  $L = 20, 24, 28$  respectively, where a MC sweep is conventionally defined as the number of moves equal to the volume of the lattice. For this reason, in order to have approximately independent configurations, we measured once every 1500 sweeps.

For each geometry, we performed long simulations at 15 different values of  $\beta$  in the disordered phase between 0.27 and 0.311, which correspond to temperatures ranging from 1.41654 to 1.63217 in units of the critical temperature for the two-dimensional Ising model  $\beta_c = \log(1 + \sqrt{2})/2 \approx 0.440687$ . For each geometry and  $\beta$  we collected approximately  $10^5$  measures. The raw data are reported in Tables 1 and 2.

The statistical variance of the observables is estimated by using the jackknife method [36]. To take into account the possible residual correlations of the samples, we used a blocking technique in the jackknife analysis. In the standard jackknife method the estimator for the variance is obtained discarding single data points. In the blocking technique, several variance estimators are considered, discarding blocks of data of increasing length and monitoring the estimated variance until it reaches a maximum.

$L$	$\xi_{12}$	$\xi_{13}$	$\chi$	$A_{13}$	$m$	$g$
$\beta = 0.3075$						
14	2.0812(17)	2.0241(12)	15.4022(79)	0.26599(25)	0.210342(60)	0.42478(49)
16	2.3396(23)	2.2947(17)	19.719(13)	0.26703(30)	0.179677(65)	0.38902(64)
18	2.5907(28)	2.5477(22)	24.273(19)	0.26740(34)	0.156237(65)	0.35715(68)
20	2.8299(40)	2.7938(30)	29.116(31)	0.26807(38)	0.137182(79)	0.32443(87)
22	3.0510(33)	3.0174(25)	33.872(28)	0.26880(31)	0.122863(55)	0.30119(79)
24	3.2719(39)	3.2349(29)	38.911(36)	0.26894(31)	0.109908(55)	0.27470(86)
28	3.6789(65)	3.6355(49)	48.776(74)	0.27097(40)	0.091858(75)	0.2360(13)
$\beta = 0.3085$						
14	2.1082(14)	2.0488(11)	15.7157(69)	0.26710(22)	0.212671(52)	0.43320(41)
16	2.3781(16)	2.3270(12)	20.2393(93)	0.26754(22)	0.182213(46)	0.39818(45)
18	2.6418(18)	2.5947(14)	25.103(12)	0.26819(22)	0.159092(42)	0.36907(47)
20	2.8958(21)	2.8542(16)	30.281(16)	0.26903(22)	0.140120(40)	0.34012(51)
22	3.1328(36)	3.0961(27)	35.514(31)	0.26992(33)	0.125993(60)	0.31663(82)
24	3.3744(39)	3.3379(30)	41.131(38)	0.27089(31)	0.113183(58)	0.29252(82)
28	3.8316(69)	3.7822(51)	52.382(80)	0.27308(40)	0.095379(79)	0.2569(13)
$\beta = 0.3000$						
14	1.8998(16)	1.8659(12)	13.3718(72)	0.26038(25)	0.194851(58)	0.37052(54)
16	2.0932(22)	2.0671(17)	16.418(11)	0.26026(31)	0.162810(61)	0.32164(73)
18	2.2586(27)	2.2420(20)	19.288(15)	0.26061(35)	0.138209(59)	0.27788(78)
20	2.4132(36)	2.3997(27)	22.069(23)	0.26093(40)	0.118453(66)	0.23766(98)
22	2.5425(33)	2.5327(24)	24.588(21)	0.26088(34)	0.103782(48)	0.20613(97)
24	2.6602(34)	2.6487(24)	26.882(23)	0.26098(32)	0.090555(42)	0.17492(97)
28	2.8636(55)	2.8495(39)	30.910(41)	0.26269(44)	0.072488(51)	0.1300(14)
$\beta = 0.3025$						
14	1.9568(16)	1.9155(12)	14.0015(73)	0.26205(25)	0.199740(58)	0.38791(52)
16	2.1682(22)	2.1408(17)	17.417(12)	0.26314(31)	0.168038(62)	0.34245(70)
18	2.3616(27)	2.3359(21)	20.789(16)	0.26247(34)	0.143824(61)	0.30275(75)
20	2.5389(37)	2.5164(28)	24.106(25)	0.26269(40)	0.124114(69)	0.26489(95)
22	2.6910(33)	2.6756(25)	27.182(24)	0.26336(34)	0.109385(51)	0.23325(95)
24	2.8355(35)	2.8220(26)	30.160(27)	0.26404(32)	0.096155(46)	0.20347(94)
28	3.0806(57)	3.0613(41)	35.373(49)	0.26494(42)	0.077706(57)	0.1565(14)
$\beta = 0.3050$						
14	2.0171(16)	1.9683(12)	14.6780(77)	0.26395(25)	0.204930(60)	0.40679(51)
16	2.2498(23)	2.2116(17)	18.515(12)	0.26418(31)	0.173660(64)	0.36476(68)
18	2.4701(28)	2.4387(21)	22.436(17)	0.26508(34)	0.149777(63)	0.32770(72)
20	2.6757(37)	2.6500(28)	26.388(27)	0.26613(38)	0.130181(72)	0.29203(89)
22	2.8641(34)	2.8364(26)	30.272(26)	0.26577(33)	0.115770(55)	0.26642(88)
24	3.0339(36)	3.0105(27)	34.042(30)	0.26624(32)	0.102440(49)	0.23553(89)
28	3.3461(65)	3.3163(48)	41.058(64)	0.26786(44)	0.083931(70)	0.1886(14)
$\beta = 0.3100$						
14	2.1460(12)	2.08097(94)	16.1664(61)	0.26787(19)	0.215981(45)	0.44418(35)
16	2.4343(12)	2.37889(90)	21.0314(69)	0.26908(16)	0.186047(34)	0.41292(31)
18	2.7193(15)	2.6677(11)	26.3595(100)	0.26998(17)	0.163321(34)	0.38646(37)
20	3.0030(17)	2.9520(13)	32.194(14)	0.27068(18)	0.144787(34)	0.36129(40)
22	3.2738(37)	3.2257(28)	38.277(33)	0.27184(33)	0.131133(62)	0.34229(79)
24	3.5552(41)	3.5032(31)	44.923(42)	0.27319(31)	0.118619(61)	0.32141(81)
28	4.0953(72)	4.0294(55)	58.956(93)	0.27539(40)	0.101535(88)	0.2944(13)
$\beta = 0.3105$						
14	2.1577(15)	2.0938(11)	16.3170(75)	0.26867(23)	0.217091(56)	0.44857(42)
16	2.4548(17)	2.3945(13)	21.297(10)	0.26921(22)	0.187326(49)	0.41820(45)
18	2.7459(20)	2.6913(15)	26.792(13)	0.27035(23)	0.164752(45)	0.39204(48)
20	3.0396(23)	2.9862(17)	32.881(18)	0.27121(23)	0.146452(44)	0.36941(52)
22	3.3226(37)	3.2667(28)	39.201(34)	0.27222(33)	0.132833(63)	0.35071(79)
24	3.6092(41)	3.5544(31)	46.245(43)	0.27320(31)	0.120487(61)	0.33219(80)
28	4.1856(73)	4.1161(55)	61.352(96)	0.27615(39)	0.103692(89)	0.3059(12)
$\beta = 0.3110$						
14	2.1746(12)	2.10673(94)	16.4952(62)	0.26906(18)	0.218364(46)	0.45238(35)
16	2.4750(17)	2.4135(13)	21.591(10)	0.26980(23)	0.188723(49)	0.42338(45)
18	2.7757(20)	2.7185(15)	27.273(13)	0.27097(23)	0.166366(45)	0.39995(47)
20	3.0736(23)	3.0208(18)	33.572(18)	0.27182(23)	0.148113(44)	0.37754(51)
22	3.3632(38)	3.3148(29)	40.241(35)	0.27305(32)	0.134690(64)	0.35948(77)
24	3.6772(41)	3.6188(32)	47.716(44)	0.27446(30)	0.122489(63)	0.34152(78)
28	4.3024(76)	4.2147(58)	64.14(10)	0.27697(39)	0.106167(93)	0.3206(12)

Table 2: Monte Carlo results.

## 5.2 Finite-size scaling and extrapolation to the infinite-volume limit

In this Section we want to test the validity of Eq. (27), by studying the FSS of the observables defined in Sec. 2. In order to compute  $F_{\mathcal{O}}(z)$ , we need to keep the ratio between the transverse sizes of two different lattices equal to  $\alpha$ . The simplest thing to do would be to take  $\alpha = 2$  but this choice has the drawback of requiring large systems: indeed, if  $L_{\perp}$  increases by a factor of two,  $L_{\parallel}$  increases by a factor of  $2^{1+\Delta} = 8$ . A more convenient choice consists in taking a noninteger  $\alpha$  almost equal to 1, as far as it is allowed by the magnitude of the relative statistical errors. This strategy requires the knowledge of the values of the observables for noninteger values of  $L_{\perp}$ . They are obtained by using an interpolation. In the analysis we used  $\alpha = 1.25$ .

At each  $\beta = \beta_a$ ,  $a = 1, \dots, n$ , our data consist of  $n^a$  triples  $(L_i^a, \xi_i^a, \mathcal{O}_i^a)$ ,  $i = 1, \dots, n^a$ , of lattices and observed values. The data points are interpolated with smooth cubic splines  $\widehat{\xi}^a(L)$ ,  $\widehat{\mathcal{O}}^a(L)$ . This interpolation provides estimates of  $\xi^a(L)$  and  $\mathcal{O}^a(L)$  for any (not necessarily integer) value of  $L$  between  $L_{\min}^a = \min_i L_i^a$  and  $L_{\max}^a = \max_i L_i^a$ . Then, we consider a set of  $m^a \equiv \lfloor (n^a + 1)/2 \rfloor$  values of  $L$ ,

$$\tilde{L}_j^a = L_{\min}^a + \frac{(j-1)}{(m^a-1)} (\alpha^{-1} L_{\max}^a - L_{\min}^a), \quad (53)$$

where  $j = 1, \dots, m^a$ , and compute the corresponding triples

$$A_j^a \equiv (z_j^a, R_{\xi,j}^a, R_{\mathcal{O},j}^a) = \left( \frac{\widehat{\xi}^a(\tilde{L}_j^a)}{\tilde{L}_j^a}, \frac{\widehat{\xi}^a(\alpha \tilde{L}_j^a)}{\widehat{\xi}^a(\tilde{L}_j^a)}, \frac{\widehat{\mathcal{O}}^a(\alpha \tilde{L}_j^a)}{\widehat{\mathcal{O}}^a(\tilde{L}_j^a)} \right) \quad (54)$$

for  $j = 1, \dots, m^a$ . The triples (54) are the data we use in the computation of the FSS functions. Note that, since we need two independent data at different values of  $L$  to compute  $R$ , we generate a number of interpolated points that is one half of the total amount of data. This minimizes the correlations among the  $A_j^a$ .

Errors are computed by using an auxiliary MC procedure that also estimates the covariance matrices  $(C_{\xi}^a)_{ij} = \text{Cov}(R_{\xi,i}^a, R_{\xi,j}^a)$  and  $(C_{\mathcal{O}}^a)_{ij} = \text{Cov}(R_{\mathcal{O},i}^a, R_{\mathcal{O},j}^a)$ .

The points  $(z_j^a, R_{\mathcal{O},j}^a)$  are fitted to  $(z, \widehat{F}_{\mathcal{O}}(z))$  where  $\widehat{F}_{\mathcal{O}}(z)$  is a polynomial in  $z$  of the form

$$\widehat{F}_{\mathcal{O}}(z) = 1 + a_{\mathcal{O},1} z^2 + a_{\mathcal{O},2} z^3 + a_{\mathcal{O},3} z^4 + \dots \quad (55)$$

Such a parametrization, different from that used in Ref. [17], is partially motivated by the theoretical results of Sec. 4, indicating that, for small  $z$ , the FSS functions behave as  $1 + az^2$ . If we neglect the correlations between  $z_j^a$  and  $R_{\mathcal{O},j}^a$ , then the  $\chi^2$  minimization is a linear problem which is easily solvable [37].

In order to detect corrections to scaling, we perform the fit several times, including in each case only the results that satisfy  $\tilde{L}_j^a \geq L_{\min, \mathcal{O}}$ , increasing step-by-step the parameter  $L_{\min, \mathcal{O}}$ .

The number  $N_{\text{par}, \mathcal{O}}$  of parameters in the fit as well as the value of  $L_{\min, \mathcal{O}}$  are chosen in such a way to optimize the values of the corresponding  $\chi^2$ . In particular, at fixed  $L_{\min, \mathcal{O}}$ , we take the value of  $N_{\text{par}, \mathcal{O}}$  which minimizes  $\chi^2/N_{\text{dof}, \mathcal{O}}$ , where  $N_{\text{dof}, \mathcal{O}}$  is the number of

$\beta$	$L_{\min} = 15.4$		$L_{\min} = 16.8$		$L_{\min} = 18.2$		$L_{\min} = 21$	
	$\xi_{\infty}$	$R^2(\text{DOF})$	$\xi_{\infty}$	$R^2(\text{DOF})$	$\xi_{\infty}$	$R^2(\text{DOF})$	$\xi_{\infty}$	$R^2(\text{DOF})$
0.27	1.6703(69)	1.2(2)	1.6671(82)	0.4(1)	1.680(12)	0.0(0)		
0.275	1.8085(84)	0.5(2)	1.8042(95)	0.3(1)	1.820(13)	0.0(0)		
0.28	1.9827(98)	0.9(2)	1.979(11)	1.0(1)	1.996(17)	0.0(0)		
0.285	2.194(11)	2.1(2)	2.189(13)	0.1(1)	2.207(20)	0.0(0)		
0.29	2.477(11)	3.1(5)	2.470(13)	3.2(4)	2.495(17)	1.3(3)	2.502(25)	0.7(2)
0.295	2.884(14)	3.8(5)	2.876(17)	2.8(4)	2.901(24)	2.2(3)	2.914(32)	0.3(2)
0.297	3.090(15)	6.1(5)	3.082(18)	5.8(4)	3.101(26)	6.2(3)	3.108(37)	6.4(2)
0.3	3.521(18)	3.9(5)	3.513(21)	4.0(4)	3.545(33)	3.6(3)	3.570(44)	2.4(2)
0.3025	4.026(21)	1.5(5)	4.012(25)	0.9(4)	4.042(38)	0.9(3)	4.069(48)	0.6(2)
0.305	4.793(25)	10(5)	4.790(30)	4.6(4)	4.816(41)	1.9(3)	4.854(58)	0.4(2)
0.3075	6.269(33)	3.4(5)	6.257(38)	3.4(4)	6.256(52)	2.4(3)	6.332(72)	0.05(2)
0.3085	7.391(38)	7.7(5)	7.390(42)	4.7(4)	7.357(58)	2.9(3)	7.464(85)	0.7(2)
0.31	11.506(94)	7.7(5)	11.49(10)	4.5(4)	11.22(13)	2.0(3)	11.60(20)	1.3(2)
0.3105	15.14(23)	12.5(5)	15.21(24)	9.2(4)	14.55(28)	5.1(3)	15.55(48)	0.1(2)

Table 3: Infinite-volume results for  $\xi_{13}$ , obtained from the extrapolation of finite-size data, for different values of  $L > L_{\min}$ .  $R^2$  is the  $\chi^2$  defined in Eq. (59), and DOF is the number of degrees of freedom.

degrees of freedom of the fit (the number of data points minus  $N_{\text{par},\mathcal{O}}$ ); then, we increase  $L_{\min,\mathcal{O}}$  until we attain  $\chi^2/N_{\text{dof},\mathcal{O}} \approx 1$  and the curve is compatible with the points with the largest value of  $L$ .

In Fig. 1 we report the FSS function  $F_{\xi}(z)$  for the correlation length  $\xi_{13}$ . The data show quite a good scaling, although at a closer look one may observe some small systematic deviations. The results of the fits are illustrated in Fig. 2. The figure is organized as follows. In the left frame we plot the residuals (the difference between the observed values and the fitting function) of the data used to perform the fit, i.e. the data points which fulfill the condition  $L \geq L_{\min,\xi}$ ; in the right frame the residual of all the data points with respect to the same fit. This is useful to detect possible systematic trends due to corrections to FSS that become smaller as the size of the system increases. The table under the frames reports the values of  $\chi^2$  and  $N_{\text{dof},\xi}$  for the fit as a function of the cut  $L_{\min,\xi}$  and of the number of parameters used  $N_{\text{par},\xi}$ .

We repeated the same analysis for  $\xi_{12}$ . As we discussed in Sec 2.2, this definition should not have a good behavior since it is not compatible with the symmetry of the low-temperature phase. This expectation is confirmed by the data, see Figs. 3 and 4: The results show strong corrections to scaling and the fitted function clearly underestimates the true  $F_{\xi}(z)$ .

Then, we considered the susceptibility as a function of  $\xi_{13}/L$ . The FSS plot is reported in Fig. 5 and the fit results in Fig. 6. The corrections to scaling are larger than those for  $\xi_{13}$ , but it is quite nice to observe that the results for the largest lattices coincide perfectly.

As a further check we consider the ratio  $A_{13}$  defined in Eq. (16). Its FSS plot is reported in Fig. 7. We observe here clear corrections to scaling that make impossible the determination of  $F_A(z)$ . Note that, if  $\gamma/\nu = 2$  as predicted by field theory, then the corrections must be nonmonotonic at least in the near-critical region. Indeed, if  $z^*$  is the critical-point constant defined in Eq. (20)—as we shall see  $z^* \approx 0.15$ —, then  $F_A(z^*) = 1$  if the exponents are the field-theoretical ones. On the contrary, our data seem to indicate

$\beta$	$L_{\min} = 15.4$		$L_{\min} = 16.8$		$L_{\min} = 18.2$		$L_{\min} = 21$	
	$\chi_{\infty}$	$R^2(\text{DOF})$	$\chi_{\infty}$	$R^2(\text{DOF})$	$\chi_{\infty}$	$R^2(\text{DOF})$	$\chi_{\infty}$	$R^2(\text{DOF})$
0.27	12.049(42)	0.8(2)	11.958(49)	1.5(1)	13.9(1.7)	0.0(0)		
0.275	13.878(51)	3.2(2)	13.759(60)	2.2(1)	16.0(2.0)	0.0(0)		
0.28	16.352(64)	0.8(2)	16.210(75)	0.4(1)	18.9(2.3)	0.0(0)		
0.285	19.714(82)	5.1(2)	19.536(96)	0.0(1)	22.8(2.8)	0.0(0)		
0.29	24.683(87)	7.9(5)	24.49(10)	5.0(4)	29.1(3.4)	1.3(3)	26.03(79)	1.3(2)
0.295	32.77(13)	9.3(5)	32.44(15)	5.6(4)	36.4(4.6)	3.0(3)	34.0(1.2)	0.8(2)
0.297	37.49(16)	15.5(5)	37.10(18)	11.1(4)	38.6(5.1)	9.3(3)	38.8(1.3)	8.7(2)
0.3	48.01(21)	5.5(5)	47.51(26)	5.8(4)	51.8(6.6)	4.0(3)	49.4(1.6)	3.7(2)
0.3025	62.06(28)	3.6(5)	61.47(33)	3.6(4)	70.0(8.7)	1.6(3)	64.3(2.1)	1.5(2)
0.305	87.02(42)	14.0(5)	86.35(48)	8.4(4)	91(12)	4.4(3)	89.8(3.0)	0.8(2)
0.3075	146.30(83)	4.8(5)	145.01(95)	4.9(4)	158(20)	3.4(3)	150.2(5.1)	0.1(2)
0.3085	201.4(1.4)	11.2(5)	200.0(1.5)	7.9(4)	211(27)	5.7(3)	205.8(7.1)	1.2(2)
0.31	474.5(7.3)	9.4(5)	472.6(7.7)	5.4(4)	504(65)	4.2(3)	478(19)	1.6(2)
0.3105	821(24)	11.8(5)	813(24)	7.8(4)	829(110)	6.4(3)	823(37)	0.4(2)

Table 4: Infinite-volume results for  $\chi$ , obtained from the extrapolation of finite-size data, for different values of  $L > L_{\min}$ .  $R^2$  is the  $\chi^2$  defined in Eq. (59), and DOF is the number of degrees of freedom.

just the opposite: Apparently  $F_A(z^*)$  is increasing with  $L$  and is larger than 1. Thus, we expect our FSS curves to be somewhat unreliable near  $z \approx z^*$ : This will be confirmed by a direct analysis that will be performed in the next Section.

Finally, we report the FSS plots for the Binder parameter, Figs. 8, 9, and for the magnetization, Fig. 10. The first one is quite good. There are tiny deviations, but they are not systematic as it can be seen from Fig. 9. The somewhat large  $\chi^2$  found in the fits is probably an indication that the statistical errors are slightly underestimated. The FSS plot of  $m$  is instead completely unreliable. At the values of  $L$  we consider, there are very large corrections to scaling and it is impossible to determine the FSS function  $F_m(z)$ .

Let us now describe the extrapolation of  $\xi$  and  $\chi$  to the infinite-volume limit.

With our preferred values of  $L_{\min}$  and  $N_{\text{par}}$  we obtain estimates of the FSS functions and then, for each triple  $(L_0, \xi_0(\beta), \chi_0(\beta)) = (L, \xi(\beta, L), \chi(\beta, L))$  obtained from the simulations we apply iteratively the map

$$\begin{pmatrix} L_n \\ \xi_n(\beta) \\ \chi_n(\beta) \end{pmatrix} = \begin{pmatrix} \alpha L_{n-1} \\ \xi_{n-1}(\beta) \hat{F}_{\xi}(\xi_{n-1}(\beta)/L_{n-1}) \\ \chi_{n-1}(\beta) \hat{F}_{\chi}(\xi_{n-1}/L_{n-1}) \end{pmatrix}, \quad (56)$$

until the asymptotic limit  $(\infty, \xi_{\infty}, \chi_{\infty}(\beta))$  is reached. Thus, for each finite-volume MC result  $\mathcal{O}(\beta, L)$ , we obtain an extrapolated value  $\mathcal{O}_{\infty}(\beta, L)$ .

To combine the estimates  $\mathcal{O}_{\infty}(\beta, L_i)$  with the same value of  $\beta$  and have a consistent estimate  $\mathcal{O}_{\infty}(\beta)$ , we proceed as in Refs. [17, 19]. We generate fake data sets, which are obtained by replacing each MC result  $\mathcal{O}$  with error  $\Delta\mathcal{O}$  by  $\mathcal{O} + r\Delta\mathcal{O}$ , where  $r$  is a normally distributed variable with zero mean and unit variance. Then, for each fake data set, using the same  $L_{\min, \mathcal{O}}$  and  $N_{\text{par}, \mathcal{O}}$ , we compute the FSS curves and perform the extrapolations. Thus, for each  $\beta$  and  $L$  that we consider in the simulation we obtain a sequence of extrapolated values  $\mathcal{O}_k^{\infty}(\beta, L)$ ,  $k = 1, \dots, M$ —typically  $M \approx 10^3$ —where  $\beta$



and  $L$  indicate that  $\mathcal{O}_k^\infty(\beta, L)$  is obtained by extrapolating the (fake) finite-volume result  $\mathcal{O}_k(\beta, L)$ . We use these results to compute the covariance of the estimates at fixed  $\beta$

$$C_{ij}(\beta) = \frac{1}{M} \sum_{k=1}^M (\mathcal{O}_k^\infty(\beta, L_i) - \mathcal{O}_\infty(\beta, L_i)) (\mathcal{O}_k^\infty(\beta, L_j) - \mathcal{O}_\infty(\beta, L_j)). \quad (57)$$

Then, we consider the weighted average

$$\widehat{\mathcal{O}}(\beta) = \frac{\sum_{i,j} (C^{-1}(\beta))_{ij} \mathcal{O}_\infty(\beta, L_j)}{\sum_{i,j} (C^{-1}(\beta))_{ij}}, \quad (58)$$

which minimizes the residual sum of squares

$$R^2(\beta) = \sum_{i,j} (C^{-1}(\beta))_{ij} (\mathcal{O}_\infty(\beta, L_i) - \widehat{\mathcal{O}}(\beta)) (\mathcal{O}_\infty(\beta, L_j) - \widehat{\mathcal{O}}(\beta)). \quad (59)$$

If the variables  $\mathcal{O}_\infty(\beta, L_i)$ ,  $i = 1, \dots, n(\beta)$ , are Gaussian with covariance  $C(\beta)$ , then  $R^2(\beta)$  is distributed as a  $\chi^2$  random variable of  $n(\beta) - 1$  degrees of freedom (DOF). Then, the deviations of  $R^2(\beta)$  from  $n(\beta) - 1$  are a measure of the consistency of the different extrapolations and  $\widehat{\mathcal{O}}(\beta)$  is our best estimate of  $\mathcal{O}_\infty(\beta)$ . The estimated error is

$$\Delta \widehat{\mathcal{O}}(\beta) = \left( \sum_{i,j} (C^{-1}(\beta))_{ij} \right)^{-1/2}. \quad (60)$$

The parameters of our preferred extrapolations are  $L_{\min} = 15.4$  and  $N_{\text{par}} = 3$  for  $\xi_{13}$  and  $L_{\min} = 18.21$  and  $N_{\text{par}} = 5$  for  $\chi$ . The corresponding FSS functions are given by

$$F_\xi(z) = 1 - 2.14297 z^2 - 171.098 z^3 + 535.11 z^4, \quad (61)$$

$$F_\chi(z) = 1 - 113.951 z^2 + 3053.15 z^3 - 38192.7 z^4 + 204378 z^5 - 394893 z^6. \quad (62)$$

The results are reported in Tables 3 and 4. All extrapolations are consistent, i.e.  $R^2(\beta) \approx n(\beta) - 1$ , except in a few isolated cases (for example the extrapolation of  $\xi_{13}$  at  $\beta = 0.3105$  for  $L_{\min} = 16.8$ ). Note also that the direct extrapolation of  $A_{13}$ —here we use the larger lattices  $L \geq 21$  to compute  $F_A(z)$ —is in good agreement with the results obtained from the extrapolated estimates of  $\chi$  and  $\xi$ , in spite of the fact that we do not have a reliable determination of  $F_A(z)$ . Clearly the errors due the neglected corrections to scaling are small compared to the extrapolation errors.

We wish finally to check the prediction (50) for the probability distribution of  $M^2$ . This cannot be done straightforwardly since we did not save the values of  $\phi(\mathbf{k}_{0,1})$  for each single configuration, but rather the sum of the values of  $\phi(\mathbf{k}_{0,1})$  for  $N = 10$  independent configurations—the ten configurations that were simulated together by our multispin program—. This means that we cannot determine from our data the distribution of  $M^2$ , but rather that of

$$\Sigma = \frac{1}{N} \sum_{i=1}^N \sigma_i \quad (63)$$

$\beta_{\min}$	$\nu$	$B_{\xi}$	$\beta_c$	$\chi^2/\text{DOF}$	DOF
0.270	0.556(15)	0.552(22)	0.31135(15)	6.1	11
0.280	0.542(13)	0.577(21)	0.31126(11)	2.8	9
0.290	0.531(11)	0.600(21)	0.311207(80)	1.3	7
0.300	0.518(15)	0.629(32)	0.311153(73)	0.53	4
0.305	0.522(56)	0.62(14)	0.31116(21)	0.91	2
0.3075	0.54(41)	0.56(93)	0.3112(13)	1.0	1

Table 5: Results for the fit (65) for several values of  $\beta_{\min}$ .

where

$$\sigma_i = \frac{M^2 L_{\parallel} L_{\perp}}{\chi}, \quad (64)$$

where the sum is over  $N$  independent systems. Since the variables  $\sigma_i$  are squares of normalized complex Gaussian random variables (see Eq. (50)),  $\Sigma$  is distributed as a reduced  $\chi^2$  variable with  $2N$  degrees of freedom (the two is due to the fact that the random variables are complex). In Figure 11 we report the distribution of  $\Sigma$  for some values of  $\beta$  and  $L$ , together with the theoretical prediction, that does not include any free parameter. As we can see the collapse is fairly good especially for the largest lattice near the critical temperature.

### 5.3 Determination of the critical indices

In order to determine the critical exponents we performed two different analyses. First, we considered the infinite-volume estimates of  $\xi_{\infty}(\beta)$  and  $\chi_{\infty}(\beta)$  and performed a fit to a power law in the reduced temperature  $t = 1 - \beta/\beta_c$ . Then, we considered the FSS behavior determining the exponents from Eqs. (21) and (23).

Let us begin with the infinite-volume correlation length  $\xi_{13}$  (in the following we simply write it as  $\xi$ ). We performed several fits of the form

$$\xi_{\infty}(\beta) = B_{\xi} t^{-\nu}, \quad (65)$$

using in each case only the estimates of  $\xi_{\infty}(\beta)$  with  $\beta \geq \beta_{\min}$ . We find the results reported in Table 5. One clearly observes the presence of corrections to scaling: The estimate of  $\nu$  decreases as  $\beta_{\min}$  increases until the fit loses predictivity. We may try to take the corrections into account, by performing a fit of the form

$$\xi_{\infty}(\beta) = B_{\xi} t^{-\nu} (1 + C_{\xi} t^{\theta}). \quad (66)$$

Since no theoretical estimate is available for the exponent  $\theta$  and our data are not precise enough to keep  $\theta$  as a free parameter, we have performed several fits, using “reasonable” values of  $\theta$ .

If we assume that the leading correction is the analytic one, i.e.  $\theta = 1$ , the fit improves substantially. The smallest value of  $\chi^2/\text{DOF}$  is attained for the lowest possible value of  $\beta_{\min}$ , i.e.  $\beta_{\min} = 0.27$ . Then, we obtain

$$\begin{aligned}\nu &= 0.4970(93), \\ \beta_c &= 0.311109(44), \\ B_\xi &= 0.693(24), \\ C_\xi &= -0.90(13),\end{aligned}\tag{67}$$

with  $(\chi^2/\text{DOF}) = 0.366$  and  $\text{DOF} = 10$ .

If we consider  $\theta = 0.5$ , we obtain again the best fit for  $\beta_{\min} = 0.27$ , yielding

$$\begin{aligned}\nu &= 0.459(16), \\ \beta_c &= 0.311058(58) \\ B_\xi &= 0.866(63) \\ C_\xi &= -0.658(92)\end{aligned}\tag{68}$$

with  $(\chi^2/\text{DOF}) = 0.526$  and  $\text{DOF} = 10$ . Note that the  $(\chi^2/\text{DOF})$  is here slightly larger than in the case  $\theta = 1$ , providing some (very weak) evidence in favor of an exponent  $\theta = 1$ .

These results indicate clearly that  $\nu \lesssim 1/2$ , with  $\nu$  decreasing with decreasing  $\theta$ . If  $\theta = 1$ , the result is perfectly compatible with the theoretical prediction (34). We also tried to see the effect of an additional analytic correction. If we consider

$$\xi_\infty(\beta) = B_\xi t^{-\nu} (1 + C_\xi t + D_\xi t^2),\tag{69}$$

we obtain for  $\beta_{\min} = 0.27$

$$\begin{aligned}\nu &= 0.501(24), \\ \beta_c &= 0.311118(73), \\ B_\xi &= 0.681(72), \\ C_\xi &= -0.75(86), \\ D_\xi &= -0.6(3.8),\end{aligned}\tag{70}$$

with  $(\chi^2/\text{DOF}) = 0.399$  and  $\text{DOF} = 9$ . As it can be seen from the errors on  $C_\xi$  and  $D_\xi$ , the addition of another fitting parameter is not justified. Our data are not precise enough to allow the determination of two correction-to-scaling terms.

Finally, assuming the theoretical prediction  $\nu = 1/2$ , we compute our best estimate of the leading correction-to-scaling exponent. We redo the fit (66), fixing  $\nu = 1/2$  and keeping  $\theta$  as a free parameter. Again, the best fit is obtained by using all data, i.e. with  $\beta_{\min} = 0.27$ . We obtain  $\theta = 1.09(22)$ ,  $\beta_c = 0.311114(28)$  with  $(\chi^2/\text{DOF}) = 0.356$  and  $\text{DOF} = 10$ . Since an analytic correction should be present, and therefore  $\theta \leq 1$ , this result confirms the analytic nature of the first correction term.

A further refinement can be obtained if we assume the theoretical prediction  $\nu = 1/2$  and  $\theta = 1$ . This provides our best estimate of the critical temperature. If we perform the

fit (66) fixing  $\nu$  and  $\theta$ , we obtain

$$\begin{aligned}\beta_c &= 0.311122(20), \\ B_\xi &= 0.6854(30), \\ C_\xi &= -0.860(46),\end{aligned}\tag{71}$$

with  $(\chi^2/\text{DOF}) = 0.35$  and  $\text{DOF} = 11$ .

We can repeat the same analysis for the susceptibility  $\chi$ . We perform a fit of the form

$$\chi_\infty(\beta) = B_\chi t^{-\gamma},\tag{72}$$

and obtain for  $\beta_{\min} = 0.27$

$$\begin{aligned}\gamma &= 0.995(34), \\ \beta_c &= 0.31118(11), \\ B_\chi &= 1.90(19),\end{aligned}\tag{73}$$

with  $(\chi^2/\text{DOF}) = 0.076$  and  $\text{DOF} = 11$ . The  $\chi^2$  is very small, indicating that probably the errors on  $\chi_\infty(\beta)$  are overestimated. The final result for  $\gamma$  is perfectly compatible with the theoretical estimate (47). Also, the estimate of  $\beta_c$  is in good agreement with the estimates of  $\beta_c$  obtained from the analysis of the correlation length. Although the goodness of the fit does not require it, we also performed a fit including an analytic correction. For  $\beta_{\min} = 0.27$ , we obtain  $\gamma = 0.98(10)$ ,  $\beta_c = 0.31116(20)$ ,  $(\chi^2/\text{DOF}) = 0.0825$  and  $\text{DOF} = 10$ . Clearly nothing changes. If we fix  $\gamma = 1$ , we obtain a more precise estimate of  $\beta_c$ . For  $\beta_{\min} = 0.27$  we have

$$\begin{aligned}\beta_c &= 0.311198(51), \\ B_\chi &= 1.877(43),\end{aligned}\tag{74}$$

with  $(\chi^2/\text{DOF}) = 0.070$  and  $\text{DOF} = 12$ . This estimate of  $\beta_c$  is in good agreement with the result (71) for the correlation length.

We have also performed a fit of the form

$$\log \chi(\beta) = a_1 \log \xi(\beta) + b_1,\tag{75}$$

that allows to determine  $a_1 = \gamma/\nu$  independently of the critical temperature. The results are reported in Table 6. There are clear corrections to scaling, with the estimates of  $a_1$  increasing towards 2 as  $\beta_{\min}$  increases. These results are perfectly consistent with what we observed before. If no correction to scaling is included, the effective  $\nu$  varies between 0.56 and 0.52 so that one would expect  $\gamma/\nu$  to vary between 1.8 and 1.9, which is exactly what we find here.

In conclusion, we find good evidence that  $\xi$  and  $\chi$  scale in the infinite-volume limit as predicted by field theory. If  $\gamma = 1$  and  $\nu = 1/2$ , we do not find evidence of nonanalytic corrections with  $\theta < 1$ . Assuming the theoretical predictions for the exponents we obtain for the critical temperature

$$\beta_c = 0.31115(10),\tag{76}$$

$\beta_{\min}$	$a_1$	$b_1$	$\chi^2/\text{DOF}$	DOF
0.270	1.856(35)	1.652(51)	0.096	12
0.280	1.867(42)	1.631(66)	0.10	10
0.290	1.883(52)	1.600(88)	0.10	8
0.300	1.899(51)	1.57(10)	0.041	5
0.305	1.921(72)	1.52(15)	0.026	3
0.3075	1.90(11)	1.58(24)	0.018	2

Table 6: Results for the fit (75) for several values of  $\beta_{\min}$ .

	$w^*$	$\gamma_{\mathcal{O}}/\nu$
$\chi$	1.543(2)	1.944(5)
$A_{13}$	1.013(1)	0.060(5)
$g$	0.902(4)	-0.46(2)
$m$	0.804(7)	-0.98(4)

Table 7: Estimates of  $\gamma_{\mathcal{O}}/\nu$  for several different observables.

where we have used the results (71) and (74). The given error is a conservative estimate that should take into account both statistical and systematic uncertainties. The result for  $\beta_c$  should be compared with the existing determinations:

$$\beta_c = \begin{cases} 0.3108(11) & \text{Ref. [38];} \\ 0.3125(13) & \text{Ref. [9].} \end{cases} \quad (77)$$

Our result (76) is in good agreement with both estimates, although much more precise.

The critical exponents can also be computed from the FSS scaling curves. First, we determine  $z^*$  by solving the equation  $\alpha = F_{\xi}(z^*)$  and by using our determination of  $F_{\xi}(z)$ . We find  $z^* = 0.1510(1)$ . Then, for each observable, we compute  $w^* = F_{\mathcal{O}}(z^*)$  and  $\gamma_{\mathcal{O}}/\nu$ , see Eq. (23). The results are reported in Table 7. For the magnetization  $m$ , cf. Eq. (9), we extrapolated the data with  $L \geq 21$ , although they are probably not asymptotic. Thus, the correct estimate of  $\beta/\nu$  could slightly decrease.

The estimate of  $\gamma/\nu$  is not far from the expected value  $\gamma/\nu = 2$ . The result is slightly lower, which may indicate that the curve varies more strongly than predicted by our naive extrapolation of the FSS curve. The reason of the difference clearly appears if we consider  $A_{13}$  whose scaling dimension is  $2 - \gamma/\nu$ . Here, we find a slightly positive value related to the already observed fact that  $F_A(z^*) \neq 1$ . Clearly for  $z \approx z^*$  there are corrections to scaling that we have not taken into account. A better analysis will be presented below.

Although our estimate of the FSS curve for  $m$  is quite bad, the result for  $\beta/\nu$  is in very good agreement with the theoretical estimate  $\beta/\nu = 1$ . Finally, let us consider the Binder parameter that apparently vanishes at the critical point as  $L^{-0.46}$ . The systematic decrease of the renormalized coupling can be seen more clearly in Fig. 12. The fact that

$L_{\min}$	$\gamma/\nu$	$Z_\chi$	$\chi^2/\text{DOF}$	DOF
14	1.975(24)	0.0902(63)	62	5
16	1.955(24)	0.0958(67)	23	4
18	1.939(27)	0.1004(77)	10	3
20	1.925(31)	0.105(10)	3.207	2
22	1.94(17)	0.101(54)	3.204	1

Table 8: Results for the fit (80) for several values of  $L_{\min}$ .

$g$  scales with a negative exponent can also be obtained with a scaling plot, by looking for  $q$  so that

$$gL^q \approx F(\xi/L). \quad (78)$$

The optimal  $q$  is  $q \approx 0.5$ , in agreement with the result of Table 7. The corresponding plot is given in Fig. 13.

It is also possible to compute the critical exponents by using the raw data near the critical point. The idea is to use Eq. (21), keeping into account the fact that our data are not exactly at  $\beta_c$ . In this case we should add a correction term and use

$$\mathcal{O}(\beta, L) = L^{\gamma/\nu} (1 + a(\beta - \beta_c)L^{1/\nu} + \dots), \quad (79)$$

where we have neglected corrections to scaling. Equation (79) is valid in the limit in which  $(\beta - \beta_c)L^{1/\nu}$  is a small correction.

We have considered our data at  $\beta = 0.311$  that are quite near to the critical point and we have performed two sets of fits. In the first fit, we have neglected the correction term in Eq. (79), by considering

$$\xi(\beta, L) = Z_\xi L^\rho, \quad \chi(\beta, L) = Z_\chi L^{\gamma/\nu}. \quad (80)$$

Using our data for  $L = 14, 16, 18, 20, 22, 24, 28$ , we have performed a series of fits, including each time only the data with  $L \geq L_{\min}$ . For  $\xi$  the results are stable with  $L_{\min}$ . The smallest  $\chi^2$  is obtained for  $L_{\min} = 18$ . Correspondingly,

$$\rho = 0.9923(85), \quad Z_\xi = 0.1544(40), \quad (81)$$

with  $\chi^2/\text{DOF} = 1.510$  and  $\text{DOF} = 3$ . This is in perfect agreement with the expected value  $\rho = 1$  and confirms the correct behavior of the correlation length. The analysis of the susceptibility gives the results reported in Table 8. They show a clear downward trend and seem to indicate that  $\gamma/\nu < 2$ . This conclusion is however incorrect. The trend is due to the fact that we have not taken into account the fact that we are not exactly at the critical point. The correction term in Eq. (79) plays an important role, as we now show. We repeat the fit by using, in accordance with Eq. (79),

$$\chi(\beta, L) = Z_\chi L^{\gamma/\nu} (1 + X_\chi L^2), \quad (82)$$

$L_{\min}$	$\gamma/\nu$	$Z_\chi$	$X_\chi$	$\chi^2/\text{DOF}$	DOF
14	2.060(43)	0.0736(77)	-0.000120(56)	9.3	4
16	2.031(80)	0.079(16)	-0.000091(90)	7.5	3
18	2.00(21)	0.086(48)	-0.00006(21)	8.7	2
20	1.9(1.1)	0.11(34)	0.0000(11)	5.78	1

Table 9: Results for the fit (82) for several values of  $L_{\min}$ . Here  $\beta = 0.311$ .

$L_{\min}$	$\gamma/\nu$	$Z_\chi$	$X_\chi$	$\chi^2/\text{DOF}$	DOF
14	2.061(50)	0.0734(82)	-0.000169(55)	10	4
16	2.037(85)	0.078(17)	-0.000147(90)	9.5	3
18	2.021(58)	0.082(12)	-0.000133(53)	13	2
20	1.9(1.2)	0.11(37)	0.0000(11)	7.9	1

Table 10: Results for the fit (82) for several values of  $L_{\min}$ . Here  $\beta = 0.3105$ .

where we have set  $\nu = 1/2$  in the correction term. The results are reported in Table 9. They are now in good agreement with the theoretical prediction  $\gamma/\nu = 2$ . The same analysis has been performed for the correlation length. Using

$$\xi(\beta, L) = Z_\xi L^\rho (1 + X_\xi L^2), \quad (83)$$

for  $L_{\min} = 20$  we obtain  $\rho = 1.000(94)$ ,  $Z_\xi = 0.1524(37)$ ,  $X_\xi = 0.00(96) \cdot 10^{-4}$  with  $\chi^2/(\text{DOF}) = 1.53$ ,  $\text{DOF} = 2$ . In this case, the addition of the correction does not change the result.

As a further check we have repeated the fit (82) by using the data at  $\beta = 0.3105$ . The results are reported in Table 10. The estimates of  $\gamma/\nu$  are in good agreement with the expected  $\gamma/\nu = 2$ . Also, the estimates of  $X_\chi$  are in rough agreement with the prediction  $X_\chi(\beta) \propto (\beta - \beta_c)$ , which implies  $X_\chi(0.3105) \approx 4X_\chi(0.3110)$ . A combined fit of the data at  $\beta = 0.311$  and  $\beta = 0.3105$  to

$$\chi(\beta, L) = L^{\gamma/\nu} (1 + Y_\chi(\beta - \beta_c)L^2), \quad (84)$$

gives, by using our estimate (76),  $\gamma/\nu = 2.032(80)$  (resp. 2.00(22)) for  $L_{\min} = 16$  (resp. 18), with  $\chi^2/\text{DOF}$  comparable to those of the previous fits. The agreement is clearly quite good.

In principle, one should also consider corrections to scaling proportional to  $L^{-\omega}$ , where we expect  $\omega \geq 2$  as a consequence of our findings  $\theta \geq 1$ . However, our data are not precise enough to allow for the determination of such a term.

## 6 Conclusions

In this paper we have performed a thorough check of the theoretical predictions for the DLG. Assuming  $\Delta = 2$ , we checked that the transverse susceptibility  $\chi$  and the transverse correlation length  $\xi_{13}$  have the correct behavior both in infinite volume for  $\beta \rightarrow \beta_c$  and at the critical point for  $L \rightarrow \infty$ . In other words, we find very good agreement with the field-theoretical predictions (34) and (40). Concerning the exponent  $\beta$ , the analysis of the magnetization at the critical point gives, although with limited precision,  $\beta \approx 1/2$ , in agreement with the field-theoretical results. It is important to notice that in all these analyses we have not found any evidence for the presence of logarithmic corrections. As it has been observed in previous studies [8], if they are really there, they are quite small.

Our result for the Binder parameter  $g$  does not agree with that of Ref. [8] where it was found  $g \neq 0$  at criticality, but confirms the results of Wang [9] that could not find a satisfactory collapse for the Binder parameter. Our result  $g = 0$  is compatible with the idea that in the scaling limit transverse correlations (both in infinite volume and in the finite-size scaling regime) are Gaussian, so that  $g = 0$  at criticality. Such a conclusion is also supported by the analysis of the distribution function of the finite-volume magnetization that is perfectly compatible with a purely Gaussian behavior. Note that this is not in contrast with the fact that  $g \neq 0$  in the low-temperature phase. Indeed, it is possible that  $g$  behaves as the magnetization, i.e.  $g \sim (T_c - T)^\zeta$  for  $T \rightarrow T_c^-$ , with  $\zeta/\nu = q \approx 0.5$ . The observed exponent  $q$  is however difficult to explain. We mention that it is also possible that  $g$  decreases as a power of  $\log L$  because of the marginal operator, but that, in our range of values of  $L$ , the complicated logarithmic dependence is mimicked by a single power. Note that, if  $g_\infty(\beta_c) = 0$ , the Binder parameter cannot be used to compute  $\beta_c$ : The crossing method does not work.

There is still a question that we don't fully understand. While the critical behavior of renormalized observables is fully in agreement with the predictions of the corresponding effective field theory, the FSS functions that we obtain for the microscopic model from our MC simulations are related to those of the coarse-grained effective field theory by the nontrivial scaling functions  $\tilde{Z}$  and  $\tilde{\tau}$  (see Eqs. (42) and (43)). In particular, the relation between the reduced temperature  $t$  of the microscopic model and the "temperature"  $\tau$  of the coarse-grained one seems to be not analytically predictable. Is this a consequence of the neglected marginal operator? An analysis of the three-dimensional case (where the operator is irrelevant), already in progress, should help us to gain a deeper understanding.

## References

- [1] S. Katz, J. L. Lebowitz, and H. Spohn, Phys. Rev. B **28**, 1655 (1983); J. Stat. Phys. **34**, 497 (1984).
- [2] For an extensive presentation of the DLG and of many generalizations, see Refs. [15, 39].
- [3] The DLG is soluble for infinite drive in the limit in which the ratio of jump rates parallel and perpendicular to the field direction becomes infinite [40].



- [4] H. K. Janssen and B. Schmittmann, *Z. Phys. B* **64**, 503 (1986).
- [5] K.-t. Leung and J. L. Cardy, *J. Stat. Phys.* **44**, 567 (1986); Erratum *J. Stat. Phys.* **45**, 1087 (1986).
- [6] The analysis of Refs. [4, 5] has been recently criticized in Refs. [41–43]. A reply to these criticisms appears in Refs. [44, 45].
- [7] M. Q. Zhang, J.-S. Wang, J. L. Lebowitz, and J. L. Vallés, *J. Stat. Phys.* **52**, 1461 (1988).
- [8] K.-t. Leung, *Int. J. Mod. Phys. C* **3**, 367 (1992).
- [9] J. S. Wang, *J. Stat. Phys.* **82**, 1409 (1996).
- [10] K.-t. Leung and J. S. Wang, *Int. J. Mod. Phys. C* **10**, 853 (1999).
- [11] K. Binder and J. S. Wang, *J. Stat. Phys.* **55**, 87 (1989).
- [12] P. L. Garrido, J. L. Lebowitz, C. Maes, and H. Spohn, *Phys. Rev. A* **42**, 1954 (1990).
- [13] G. Grinstein, *J. Appl. Phys.* **69**, 5441 (1991).
- [14] J. L. Vallés and J. Marro, *J. Stat. Phys.* **43**, 441 (1986); **49**, 89 (1987).
- [15] B. Schmittmann and R. P. K. Zia, Statistical mechanics of driven diffusive systems, in *Phase Transitions and Critical Phenomena*, edited by C. Domb and J. L. Lebowitz, Vol. 17 (Academic Press, London, 1995).
- [16] S. Caracciolo, A. Gambassi, M. Gubinelli, and A. Pelissetto, *Eur. Phys. J. B* **20**, 255 (2001), e-print [cond-mat/0010479](#).
- [17] S. Caracciolo, R. G. Edwards, S. J. Ferreira, A. Pelissetto, and A. D. Sokal, *Phys. Rev. Lett.* **74**, 2969 (1995), e-print [hep-lat/9409004](#).
- [18] A similar method has been introduced in Refs. [46, 47].
- [19] S. Caracciolo, R. G. Edwards, A. Pelissetto, and A. D. Sokal, *Phys. Rev. Lett.* **75**, 1891 (1995), e-print [hep-lat/9411009](#).
- [20] S. Caracciolo, R. G. Edwards, T. Mendes, A. Pelissetto, and A. D. Sokal, *Nucl. Phys. B (Proc. Suppl.)* **47**, 763 (1996), e-print [hep-lat/9509033](#).
- [21] G. Mana, A. Pelissetto, and A. D. Sokal, *Phys. Rev. D* **54**, 1252 (1996), e-print [hep-lat/9602015](#).
- [22] T. Mendes, A. Pelissetto, and A. D. Sokal, *Nucl. Phys. B* **477**, 203 (1996), e-print [hep-lat/9604015](#).
- [23] G. Mana, A. Pelissetto, and A. D. Sokal, *Phys. Rev. D* **55**, 3674 (1997), e-print [hep-lat/9610021](#).

- [24] S. J. Ferreira and A. D. Sokal, J. Stat. Phys. **96**, 461 (1999), e-print cond-mat/9811345.
- [25] S. Caracciolo and M. Palassini, Phys. Rev. Lett. **82**, 5128 (1999), e-print cond-mat/9904246.
- [26] K. Kawasaki, in *Phase Transitions and Critical Phenomena*, edited by C. Domb and M. S. Green, Vol. 2, p. 443 (Academic Press, New York, 1972).
- [27] In principle, it is enough to consider periodic boundary conditions in the field direction. The boundary conditions in the transverse directions are largely irrelevant for the problems discussed here.
- [28] A field theory for the DLG was also derived in Ref. [48], starting from the standard Model-B dynamics. The external drive partially breaks the supersymmetry (SUSY) of Model B, giving rise to a crossover towards a new fixed point in  $d = 5$ , with a residual symmetry ( $\frac{1}{2}$ SUSY of Ref. [48]).
- [29] We must note that the susceptibility defined by using the linear response theory does not coincide in general non-equilibrium system with that defined in terms of the Fourier transform of the two-point correlation function.
- [30] H. K. Janssen, Z. Phys. B **23**, 377 (1976).
- [31] R. Bausch, H. K. Janssen, and H. Wagner, Z. Phys. B **24**, 113 (1976).
- [32] H. K. Janssen, Field-theoretic method applied to critical dynamics, in *Dynamical Critical Phenomena and Related Topics*, edited by C. P. Enz, Lecture Notes in Physics, Vol. 104, (Springer, Berlin–New York–Tokyo, 1979).
- [33] J. Zinn-Justin, *Quantum Field Theory and Critical Phenomena*, 3 ed. (Oxford Science Publication, Clarendon Press, Oxford, 1996).
- [34] E. Brézin, J. Physique **43**, 15 (1982).
- [35] D. E. Knuth, *The Art of Computer Programming, Vol. 2 - Seminumerical Algorithms* (Addison-Wesley, Reading, Massachusetts, 1997).
- [36] B. Efron, *The Jackknife, the Bootstrap and Other Resampling Plans*, Regional Conference Series in Applied Mathematics, Vol. 38 (SIAM, Philadelphia, 1982).
- [37] Not any basis in the space spanned by the functions  $\{z^k\}$  is suitable to perform the fit. As discussed in Ref. [23], care must be taken to choose functions which are effectively orthogonal with respect to the scalar product induced by the  $\chi^2$ , otherwise the numerical solution of the minimization problem can be unstable. We used the functions  $f_k(z) = z^2 P_{k-1}^{(6,2)}(2z/z_{\max} - 1)$ , where  $P_n^{(a,b)}$  are Jacobi polynomials which are an orthonormal system in  $L^2([0, 1], x^a(1-x)^b)$ . The constant  $z_{\max}$  must be such that  $z_{\max} > z_j^a$  for all  $a, j$ . We chose  $z_{\max} = 0.16$ . The choice of the parameters  $a, b$  is not crucial and different choices would perform analogously.

- [38] K.-t. Leung, Phys. Rev. Lett. **66**, 453 (1991).
- [39] J. Marro and R. Dickman, *Nonequilibrium Phase Transitions in Lattice Models* (Cambridge University Press, Cambridge, 1999).
- [40] H. van Beijeren and L. S. Schulman, Phys. Rev. Lett. **53**, 806 (1984).
- [41] P. L. Garrido, F. de los Santos, and M. A. Muñoz, Phys. Rev. E **57**, 752 (1998).
- [42] P. L. Garrido and F. de los Santos, J. Stat. Phys. **96**, 303 (1999), e-print cond-mat/9805211.
- [43] P. L. Garrido, M. A. Muñoz, and F. de los Santos, Phys. Rev. E **61**, R4683 (2000), e-print cond-mat/0001165.
- [44] B. Schmittmann, H. K. Janssen, U. C. Täuber, R. K. P. Zia, K.-t. Leung, and J. L. Cardy Phys. Rev. E **61**, 5977 (2000), e-print cond-mat/9912286.
- [45] K.-t. Leung, Phys. Rev. E **63**, 016102 (2001), e-print cond-mat/0006217.
- [46] M. Luscher, P. Weisz, and U. Wolff, Nucl. Phys. B **359**, 221 (1991).
- [47] J.-K. Kim, Europhys. Lett. **28**, 211 (1994); Phys. Rev. D **50**, 4663 (1994); Nucl. Phys. B (Proc. Suppl.) **34**, 702 (1994).
- [48] K. Gawedzki and A. Kupiainen, Nucl. Phys. B **269**, 45 (1986).

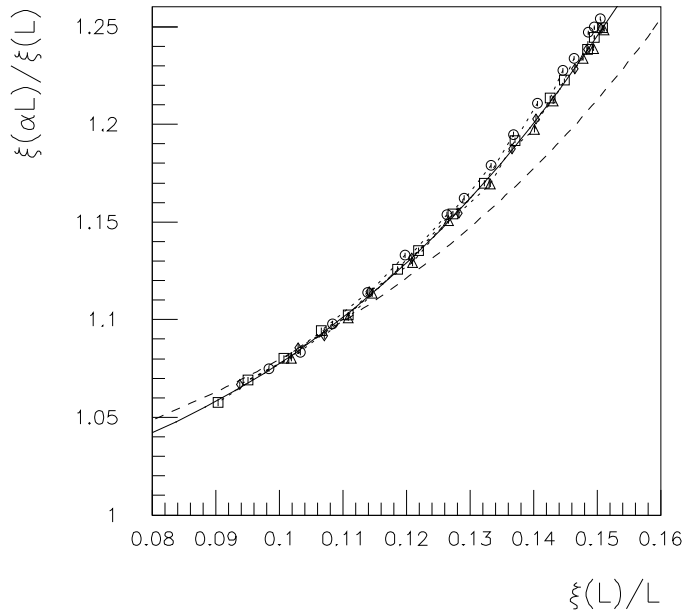
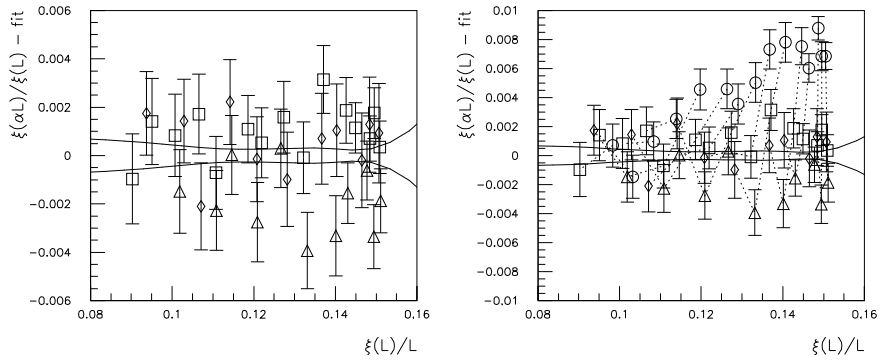


Figure 1: FSS plot for  $\xi_{13}$  versus  $\xi_{13}$ . The symbols correspond to the following lattice sizes: ( $\circ$ )  $L \leq 15$ , ( $\square$ )  $15 < L \leq 17$ , ( $\triangle$ )  $17 < L \leq 22$ , ( $\diamond$ )  $L > 22$ . Dotted lines connect data at the same temperatures. The dashed line is the approximation (46), the continuous line is the result of the fit with  $L_{\min} = 15.4$ .



$L_{\min}$	$N_{\text{par}}$	$\chi^2$	$N_{\text{dof}}$	$\chi^2/N_{\text{dof}}$
14	3	286	49	5.8
15.4	3	39	34	1.1
16.8	3	36	30	1.2
18.2	3	22	19	1.1
21	3	4.5	8	0.6

Figure 2: Fit of the FSS function of  $\xi_{13}$  versus  $\xi_{13}$ . The symbols correspond to the following lattice sizes: ( $\circ$ )  $L \leq 15$ , ( $\square$ )  $15 < L \leq 17$ , ( $\triangle$ )  $17 < L \leq 22$ , ( $\diamond$ )  $L > 22$ . Dotted lines connect data at the same temperature. In the left frame only the data used in the fit are plotted, while in the right frame all the data are showed. The solid lines give the estimated error on the fitted function (one standard deviation). The graphs correspond to  $L_{\min} = 15.4$ .

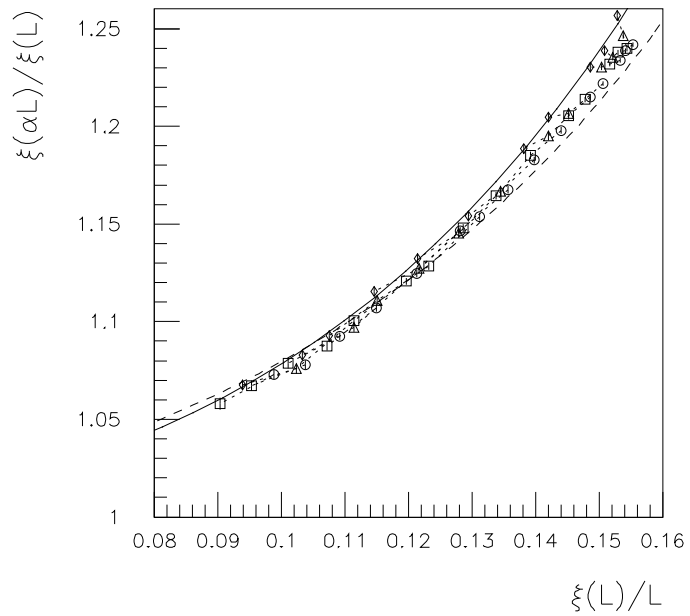
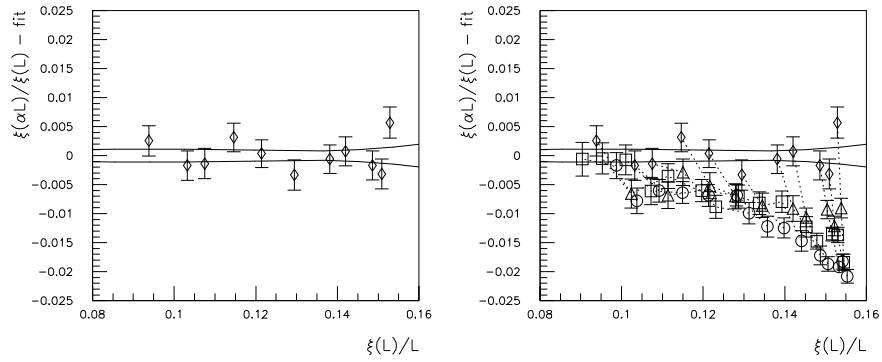


Figure 3: FSS plot for  $\xi_{12}$  versus  $\xi_{12}$ . The symbols correspond to the following lattice sizes: ( $\circ$ )  $L \leq 15$ , ( $\square$ )  $15 < L \leq 17$ , ( $\triangle$ )  $17 < L \leq 22$ , ( $\diamond$ )  $L > 22$ . Dotted lines connect data at the same temperatures. The dashed line is the approximation (46), the continuous line is the result of the fit with  $L_{\min} = 21$ .



$L_{\min}$	$N_{\text{par}}$	$\chi^2$	$N_{\text{dof}}$	$\chi^2/N_{\text{dof}}$
14	3	277	49	5.6
15.4	3	142	34	4.2
16.8	3	140	30	4.6
18.2	3	83	19	4.4
21	3	10	8	1.3

Figure 4: Fit for the FSS function of  $\xi_{12}$  versus  $\xi_{12}$ . The symbols correspond to the following lattice sizes: ( $\circ$ )  $L \leq 15$ , ( $\square$ )  $15 < L \leq 17$ , ( $\triangle$ )  $17 < L \leq 22$ , ( $\diamond$ )  $L > 22$ . Dotted lines connect data at the same temperature. In the left frame only the data used in the fit are plotted, while in the right frame all the data are showed. The solid lines give the estimated error on the fitted function (one standard deviation). The graphs correspond to  $L_{\min} = 21$ .

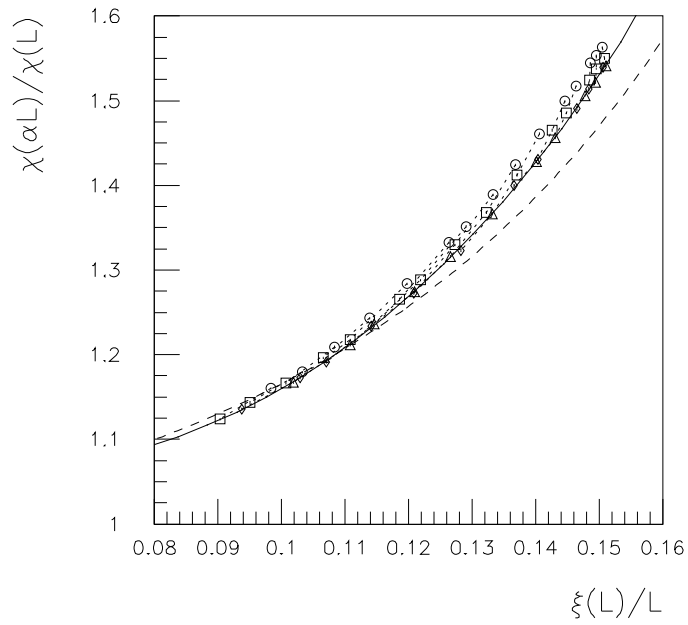
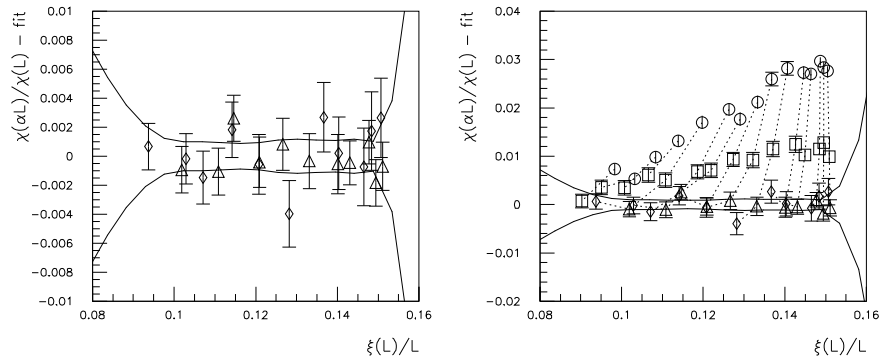


Figure 5: FSS plot for  $\chi$  versus  $\xi_{13}$ . The symbols correspond to the following lattice sizes: ( $\circ$ )  $L \leq 15$ , ( $\square$ )  $15 < L \leq 17$ , ( $\triangle$ )  $17 < L \leq 22$ , ( $\diamond$ )  $L > 22$ . Dotted lines connect data at the same temperatures. The dashed line is the approximation (47), the continuous line is the result of the fit with  $L_{\min} = 18.2$ .





$L_{\min}$	$N_{\text{par}}$	$\chi^2$	$N_{\text{dof}}$	$\chi^2/N_{\text{dof}}$
14	3	2121	49	43
15.4	3	224	34	6.6
16.8	3	208	30	6.9
18.2	5	13	17	0.78
21	4	6.5	7	0.93

Figure 6: Fit of the FSS function of  $\chi$  versus  $\xi_{13}$ . The symbols correspond to the following lattice sizes: ( $\circ$ )  $L \leq 15$ , ( $\square$ )  $15 < L \leq 17$ , ( $\triangle$ )  $17 < L \leq 22$ , ( $\diamond$ )  $L > 22$ . Dotted lines connect data at the same temperature. In the left frame only the data used in the fit are plotted, while in the right frame all the data are showed. The solid lines give the estimated error on the fitted function (one standard deviation). The graphs correspond to  $L_{\min} = 18.2$ .

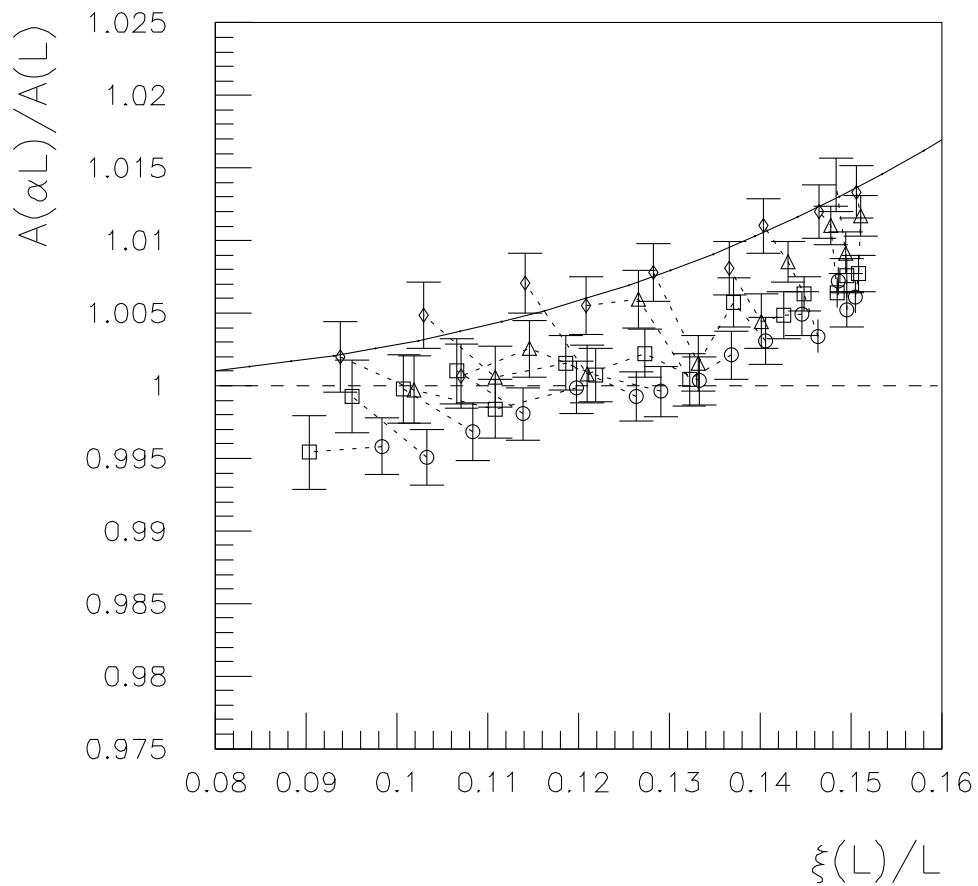


Figure 7: FSS plot for  $A_{13}$  versus  $\xi_{13}$ . The symbols correspond to the following lattice sizes: ( $\circ$ )  $L \leq 15$ , ( $\square$ )  $15 < L \leq 17$ , ( $\triangle$ )  $17 < L \leq 22$ , ( $\diamond$ )  $L > 22$ . Dotted lines connect data at the same temperatures. The continuous line is the result of the fit with  $L_{\min} = 21$ .

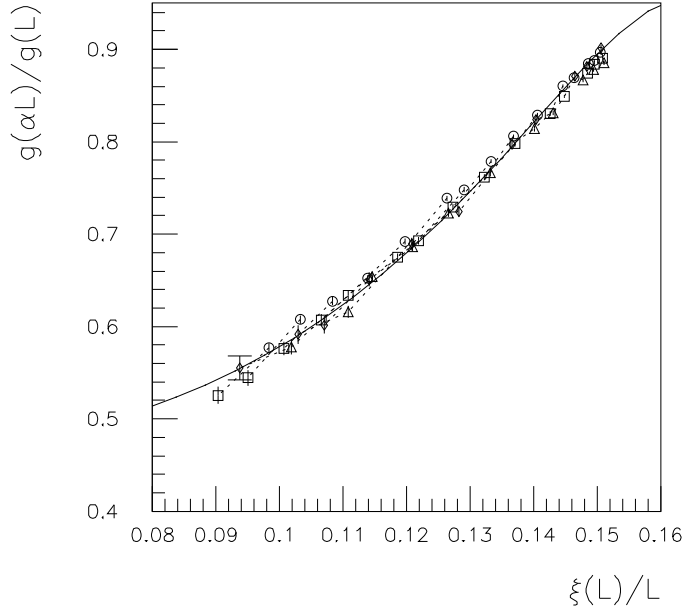
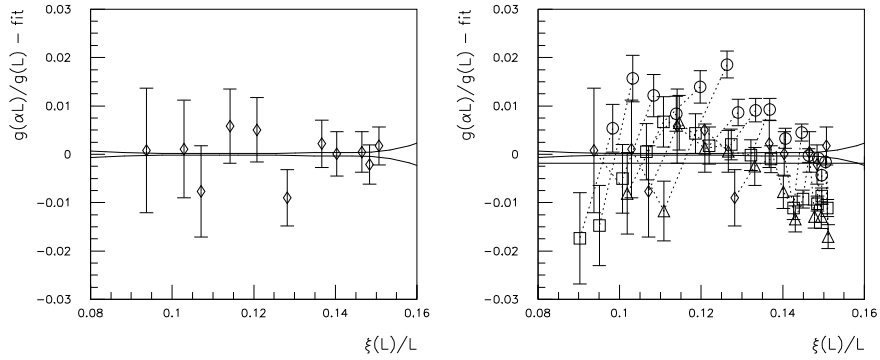


Figure 8: FSS plot for  $g$  versus  $\xi_{13}$ . The symbols correspond to the following lattice sizes: ( $\circ$ )  $L \leq 15$ , ( $\square$ )  $15 < L \leq 17$ , ( $\triangle$ )  $17 < L \leq 22$ , ( $\diamond$ )  $L > 22$ . Dotted lines connect data at the same temperatures. The continuous line is the result of the fit with  $L_{\min} = 21$ .



$L_{\min}$	$N_{\text{par}}$	$\chi^2$	$N_{\text{dof}}$	$\chi^2/N_{\text{dof}}$
14	3	260	49	5.3
15.4	3	56	34	1.7
16.8	3	56	30	1.9
18.2	3	47	19	2.5
21	4	4.7	7	0.68

Figure 9: Fit of the FSS function of  $g$  versus  $\xi_{13}$ . The symbols correspond to the following lattice sizes: ( $\circ$ )  $L \leq 15$ , ( $\square$ )  $15 < L \leq 17$ , ( $\triangle$ )  $17 < L \leq 22$ , ( $\diamond$ )  $L > 22$ . Dotted lines connect data at the same temperature. In the left frame only the data used in the fit are plotted, while in the right frame all the data are showed. The solid lines give the estimated error on the fitted function (one standard deviation). The graphs correspond to  $L_{\min} = 21$ .

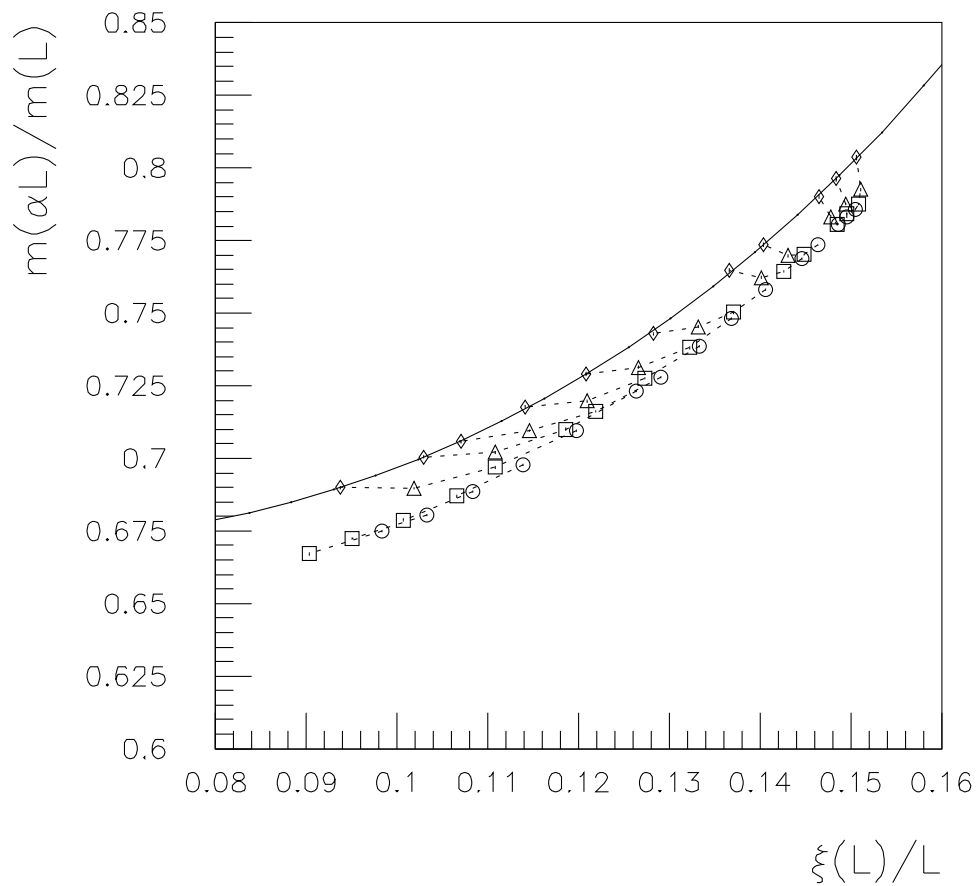


Figure 10: FSS plot for  $m$  versus  $\xi_{13}$ . The symbols correspond to the following lattice sizes: ( $\circ$ )  $L \leq 15$ , ( $\square$ )  $15 < L \leq 17$ , ( $\triangle$ )  $17 < L \leq 22$ , ( $\diamond$ )  $L > 22$ . Dotted lines connect data at the same temperatures. The continuous line is the result of the fit with  $L_{\min} = 21$ .

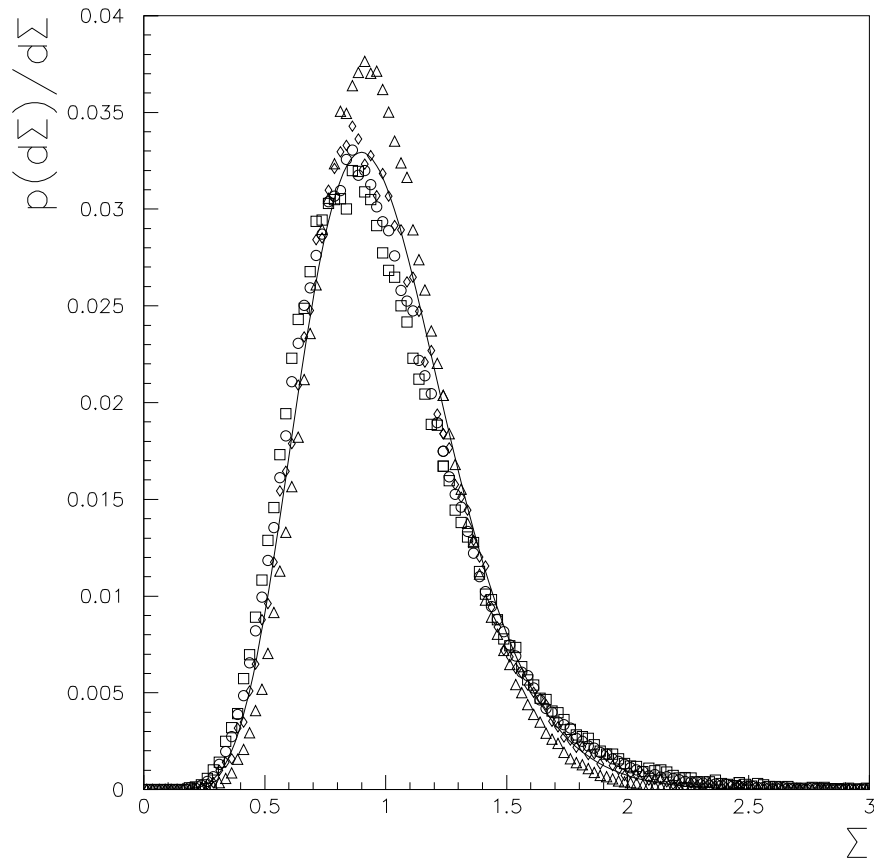


Figure 11: Distribution function of the variable  $\Sigma$ . The symbols refer to different values of  $\beta$  and  $L$ :  $\circ$  ( $\beta = 0.27, L = 16$ ),  $\square$  ( $\beta = 0.29, L = 28$ ),  $\triangle$  ( $\beta = 0.311, L = 16$ ),  $\diamond$  ( $\beta = 0.311, L = 28$ ). The solid line is the theoretical prediction as discussed in the text.

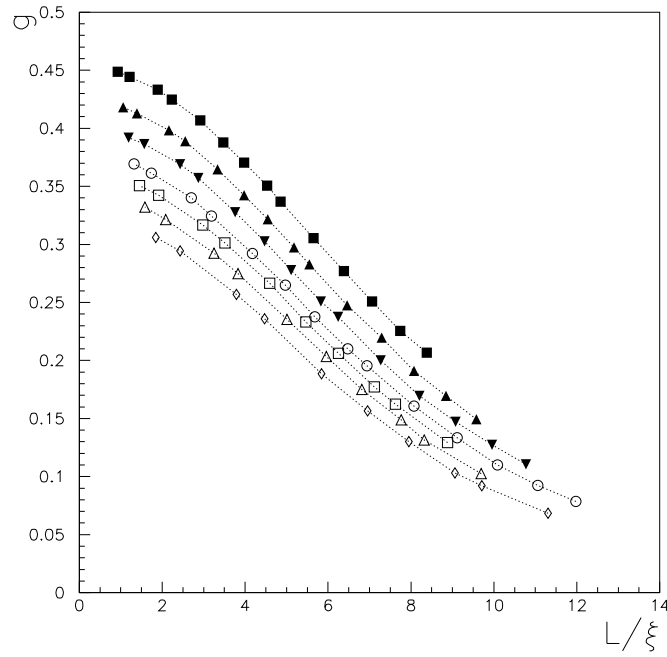


Figure 12: Binder cumulant:  $g$  versus  $\xi_{13}/L$ . The symbols correspond to the following lattice sizes:  $L= 14(\blacksquare)$ ,  $16(\blacktriangle)$ ,  $18(\blacktriangledown)$ ,  $20(\circ)$ ,  $22(\square)$ ,  $24(\triangle)$ ,  $28(\diamond)$ .

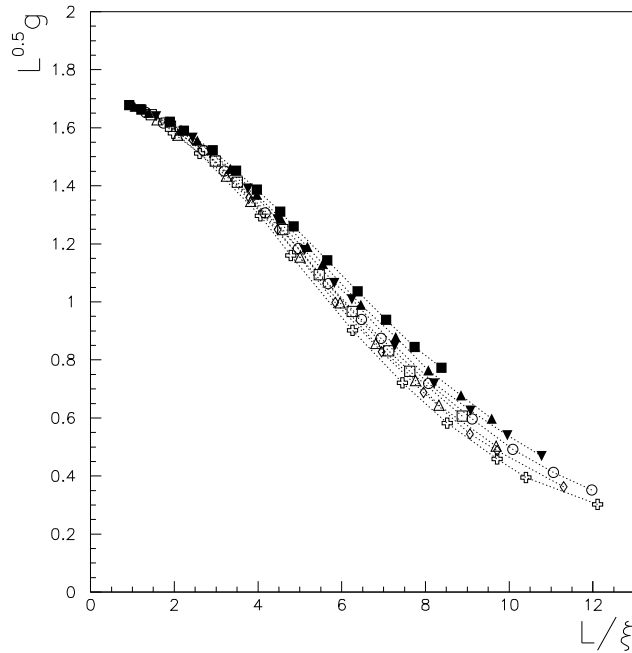


Figure 13: Rescaled Binder cumulant:  $L^{0.5}g$  versus  $\xi_{13}/L$ . The symbols correspond to the following lattice sizes:  $L= 14(\blacksquare)$ ,  $16(\blacktriangle)$ ,  $18(\blacktriangledown)$ ,  $20(\circ)$ ,  $22(\square)$ ,  $24(\triangle)$ ,  $28(\diamond)$ .